Sedimentary Geology 301 (2014) 70–89

Contents lists available at ScienceDirect

Sedimentary Geology

journal homepage: www.elsevier.com/locate/sedgeo

Alluvial fan deposition along a rift depocentre border from the Neuquén Basin, Argentina

Martin Muravchik *, Andrés Bilmes, Leandro D'Elia, Juan R. Franzese

Centro de Investigaciones Geológicas, Universidad Nacional de La Plata-CONICET, Calle 1 #644, B1900TAC, La Plata, Argentina

ARTICLE INFO

Article history:
Received 25 September 2013
Received in revised form 27 December 2013
Accepted 28 December 2013
Available online 4 January 2014

Editor: J. Knight

Keywords:
Alluvial processes
Structural controls
Alluvial fan orientation
Syn-rift
Neuquén Basin

ABSTRACT

The interaction between hangingwall block rotation and alluvial deposition is examined from Late Triassic–Early Jurassic successions exposed along the Catán Lil half-graben border fault system in the Neuquén Basin, Argentina. Analysis of transport and depositional processes, clast composition and rock body geometry allowed the identification of three distinctive fan-shaped alluvial units. The contrasting lithologic nature of the basement (igneous-metamorphic) and syn-rift fill (volcanic and volcanic-derived) permits detailed studies of clast provenance. The origin of each alluvial system (footwall- vs. hangingwall-derived) can thus be verified. A simple method was implemented to establish the geometry of each alluvial unit by comparing the stereographic projection of its bedding to that of an idealised fan shaped body. Results show that the three alluvial systems occupied the same relative location in the rift depocentre. Unit 1 is interpreted as an alluvial fan orientated transverse to the depocentre border fault system and fed from the footwall. Non-cohesive debris flow deposition was the dominant process in this environment. Unit 2 is interpreted as a mainly hangingwall-fed alluvial fan, parallel to the depocentre border fault system and shows an upward decrease in footwall-derived clasts. Hyperconcentrated flow was the principal transport process. Unit 3 represents a fan delta, parallel to the depocentre border fault system. Its components are completely hangingwall-derived and hyperconcentrated flow deposition was the dominant process. Differences in grain-size, composition, transport directions and fan body geometry are proved to be directly linked to variations in ground tilting induced by the direction of hangingwall block rotation in an endorheic rift depocentre.

1. Introduction

Most of the published examples of alluvial evolution along border fault systems result from studies undertaken in rift depocentres limited by strongly interacting fault segments over relatively well integrated drainage networks (e.g., Alexander and Leeder, 1987; Jackson and Leeder, 1994; Eliet and Gawthorpe, 1995; Leeder et al., 1996; Leeder and Mack, 2001). Linkage of small fault segments into large border fault systems controls the location, size and shape of footwall catchments and the focusing of sediment supply to hangingwall depocentres (e.g., Roberts and Jackson, 1991; Gawthorpe and Hurst, 1993; Leeder and Jackson, 1993), favouring the inception of alluvial systems orientated either transverse or parallel to the fault scarps (e.g. Gawthorpe et al., 1994; Eliet and Gawthorpe, 1995; Leeder et al., 1996; Cowie et al., 2006). As a result, well established depocentre- to basin-scale predictive models of alluvial evolution in rift basins already exist (e.g., Eliet and Gawthorpe, 1995; Gawthorpe and Leeder, 2000; Cowie et al., 2006). In contrast, more detailed scale models are still needed in order to understand the evolution of individual fans and the local controls operating over them. The work presented in this study documents the evolution of alluvial units in a presumably hydrologically-closed depocentre next to a border fault system in which fault segments were already linked. This isolated condition prevented the development of axial fluvial systems connecting different depocentres and interacting with any transverse alluvial system elements (e.g., Mack and Leeder, 1999; Leeder and Mack, 2001). In the absence of propagating and linking fault segments along the border fault system, differences in hangingwall block rotation and subsidence were the main control over alluvial fan/fan delta configuration and orientation. Some of these characteristics are addressed as being originated from deforming a more competent hangingwall substrate as opposed to rift basin situations where the deforming hangingwall substrate is composed of relatively thick unconsolidated syn-rift sediments and/or sedimentary rock pre-rift units. The main objective of this contribution is to evaluate the evolution of an alluvial environment originated along a half-graben border, in terms of changes in fan geometry and orientation, source areas and sedimentary processes, and how the integration of these parameters can be used in order to understand the effects of ground tilting and hangingwall block rotation. The data used for this purpose come from the analysis of an inverted and eroded fossil rift depocentre and the interpretations are based on its reconstructed fill.

* Corresponding author at: Department of Earth Science, University of Bergen, Allégaten 41, N-5007, Bergen, Norway. Tel.: +47 555 83294.
E-mail addresses: martin.muravchik@geo.uib.no (M. Muravchik), abilmes@cig.museo.unlp.edu.ar (A. Bilmes), ldelia@cig.museo.unlp.edu.ar (L. D'Elia), franzese@cig.museo.unlp.edu.ar (J.R. Franzese).

0037-0738/$ – see front matter © 2014 Elsevier B.V. All rights reserved.
http://dx.doi.org/10.1016/j.sedgeo.2013.12.007

The methodology used and the results obtained from the present analysis are expected to be of general applicability to other similar areas and can contribute to the generation of predictive models of potential use in the mineral and oil industries.

2. Geological setting

The Neuquén Basin is located between latitudes 32° and 40°S, mainly in west-central Argentina but also extending west into Chile (Fig. 1A). The basin has a triangular shape, occupying an area of about 160,000 km^2, and the basin fill stratigraphy extends from the Early Triassic to Holocene, with a maximum thickness of at least 7000 m (Vergani et al., 1995). The origin of the basin lies in pre-Andean extensional processes related to the extensional collapse of the Gondwanic Orogen (Uliana and Legarreta, 1993; Tankard et al., 1995; Vergani et al., 1995; Franzese and Spalletti, 2001), and its evolution can be divided into three phases: a rift phase (Late Triassic–Early Jurassic), a post-rift phase (Early Jurassic–Early Cretaceous) and a foreland phase (Late Cretaceous–Cenozoic) (Uliana and Legarreta, 1993; Tankard et al., 1995; Vergani et al., 1995; Franzese and Spalletti, 2001; Howell et al., 2005).

Long, narrow, isolated depocentres formed during Late Triassic to Early Jurassic rifting (Fig. 1A,B), accompanied by intense magmatic activity. The syn-rift basin fill can be divided into a lower Precuyano Cycle (Gulisano et al., 1984) and an upper Cuyano Cycle (Groeber, 1946) (Fig. 2). The Precuyano Cycle comprises a complex array of mainly continental volcanic and sedimentary (alluvial, fluvial and lacustrine) deposits (Franzese and Spalletti, 2001; Franzese et al., 2006, 2007; Muravchik et al., 2011; D'Elia et al., 2012; D'Elia and Martí, 2013). Marine clastic and carbonate rocks of the Precuyano Cycle are present in Chile and locally in Argentina (Riccardi et al., 1997; Lanés, 2005; Giambiagi et al., 2008). The Cuyano Cycle units represent a widespread marine transgression that diachronously flooded the entire Neuquén Basin in a southward direction from the Late Triassic through the Early Jurassic (Pliensbachian). It comprises relatively thin conglomerates and shallow marine carbonate deposits followed by very thick (at least 1000 m) black shale deposits with some intercalated sandstones (e.g., Gulisano, 1981; Gulisano and Pando, 1981; Legarreta and Uliana, 1996).

3. Study area

This work focuses on alluvial deposits from the syn-rift Precuyano Cycle and their transition to the Cuyano Cycle in the Catán Lil Depocentre (Fig. 1). Exposures lie along the Catán Lil and Chachil ranges, about 70 km southwest of the city of Zapala, where outcrops of basement rocks and syn-rift successions are well preserved (Figs. 1, 3). The basement includes Permian–Carboniferous granitoids of the Chachil Plutonic Complex (Leanza, 1990) intruding Siluro-Devonian schists of the Piedra Santa Formation (Digregorio and Uliana, 1980) (Figs. 2, 3A). The initial syn-rift fill is represented by the Lapa Formation (Groeber, 1956) (Precuyano Cycle) consisting of lava flows, alluvial, pyroclastic and reworked pyroclastic deposits (Groeber, 1956; Leanza, 1990; Franzese and Spalletti, 2001; Franzese et al., 2006, 2007). Black shale deposits of the Los Molles Formation (Weaver, 1931, in Leanza, 1990) (Cuyano Cycle) completely cover all older units in the area.

The Catán Lil Depocentre (Fig. 3) is elongated in a northwest–southeast direction and is now completely bordered by inverted normal fault systems in two sets; one trending northwest–southeast and another trending northeast–southwest (Muravchik, 2009), defining a more or less rectangular hangingwall depocentre in plan view

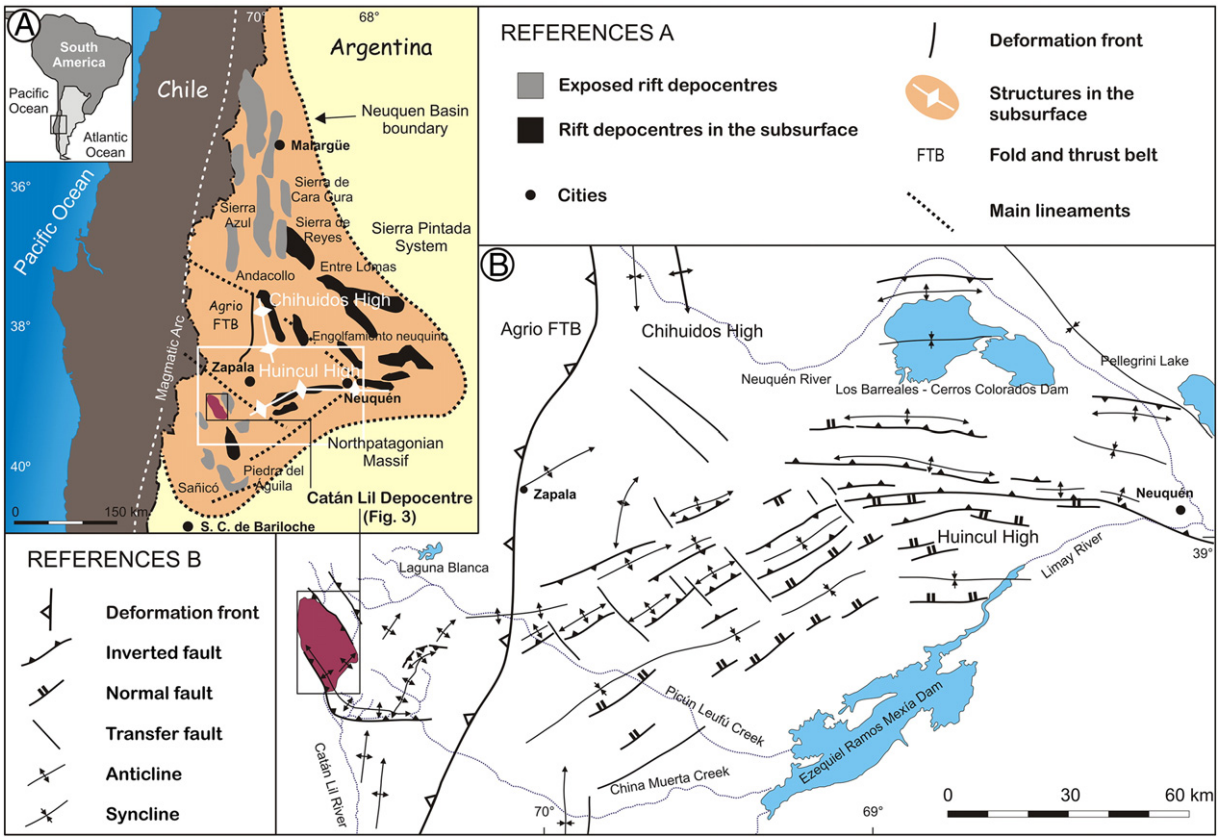

Fig. 1. Location map of the study area. (A) Distribution of rift depocentres in the Neuquén Basin, Argentina. The white rectangle shows the extent of (B). Modified from Franzese and Spalletti (2001). (B) Map of the major structures in southern Neuquén Basin. Location of the Catán Lil Depocentre is highlighted with a black rectangle. Structures from the Huincul High are according to Vergani (2005).

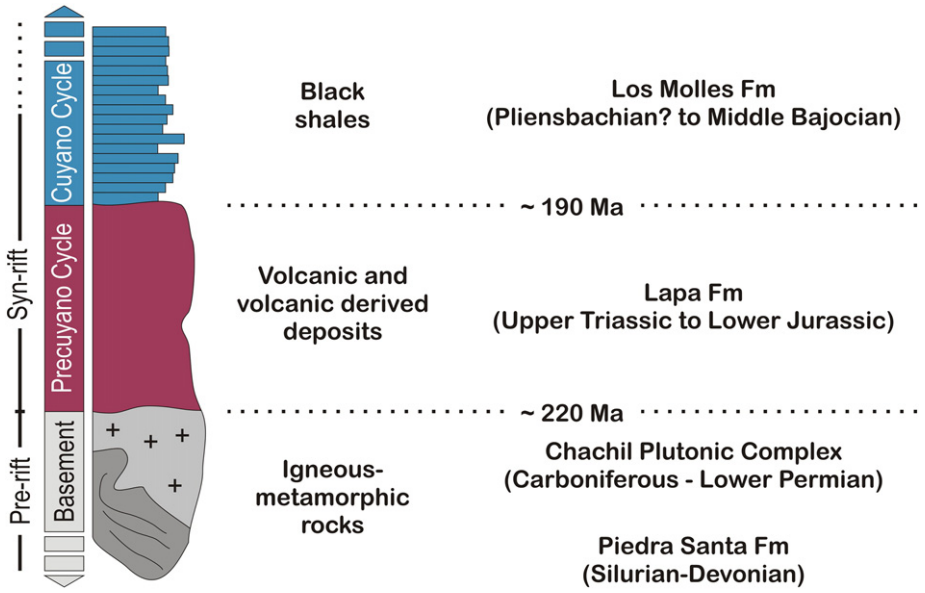

Fig. 2. Schematic stratigraphic column representing the different units that integrate the Catán Lil Depocentre, Neuquén Basin.

(Fig. 3A). Although extensional structures that formed during the Late Triassic–Early Jurassic rifting have been variably inverted, the geometry of the original rift depocentre can still readily be reconstructed by stratigraphic correlation of the syn-rift units (Fig. 3B). The depocentre is interpreted as a half-graben based on the asymmetry of its fill (e.g., Leeder and Gawthorpe, 1987; Gawthorpe and Leeder, 2000): the thickest syn-rift accumulations are found along the northeastern border fault system while the thinnest occur along the southwestern border (Fig. 3B). Therefore, the northeastern border fault system is considered to be where normal faults accrued their greatest displacement. The corresponding northeastern footwall block has a horst geometry, is ~5 km across strike and delimits a contiguous rift depocentre (Fig. 3A). Other studies in the area indicate that the two fault systems at either side of the horst were active at the same time, so this block constituted a high relief area for both depocentres (Franzese et al., 2006; Muravchik, 2009).

The studied alluvial succession crops out next to the northeastern border fault system, overlying lava flow units and overlain by black shale marine deposits of the Cuyano Cycle (Fig. 4). The lava flow units constitute an amalgamated succession approximately 1000 m thick of andesites and dacites. Examination of the lava succession at other localities situated to the northwest and the southeast along the northeastern border fault system (Fig. 3A) reveals great consistency in thickness (Muravchik, 2009). It is crucial to note the role of the composition of the fault blocks in the style of the deformation observed in this depocentre. The current fault blocks, mainly consisting of granitoids with a thick layer of consolidated lava flows (several hundreds of metres thick), can only behave as discrete rigid mechanical units. No internal deformational structures such as anticline, syncline or monocline folding (i.e., distributed deformation) are detected within the fault blocks (Fig. 3A). Likewise, neither drag folds nor monocline folds are observed associated with the borders of these fault blocks. Folding is restricted to the less competent lithologies that compose the Cuyano Cycle (Fig. 3A). Therefore, the presence of topographic gradients in the hangingwall area after the deposition of the lava flow units is interpreted to be the result of either ground-tilting caused by rotation of the fault blocks or a pre-existing volcanic topography. The lack of transverse structures (i.e., folds or faults) affecting either the lava flow units or the alluvial succession along the northeastern border fault system (Fig. 3A) indicates that no linkage of fault segments occurred after the emplacement of the lava flows (Schlische, 1992; Anders and Schlische, 1994; Schlische and Anders, 1996; Morley, 1999, 2002). This observation together with the relatively constant thickness developed by the lava flow units along the current fault system suggests that the northeastern border fault system had already been linked by the time that deposition of the alluvial units began. The alluvial succession consists of three units – Units 1 (oldest), 2 and 3 (youngest) – readily distinguishable in the field by means of grain size, sedimentary structures and clast provenance.

4. Methodology

Detailed geologic mapping, sedimentary logging and facies analysis were performed in order to determine the main depositional characteristics of the alluvial units. Six log sections were logged at 1:100 scale. The geometry of the three syn-rift alluvial units was studied by constructing 2D cross sections parallel to the border fault system and by stereographic projection techniques. The latter consists in plotting the bedding dip and dip direction in a stereographic projection and comparing it with that of a theoretical cone projection (Fig. 5). If the measurements are taken over the same surface of a cone (Fig. 5A) the results will show the data uniformly distributed along a small circle (Fig. 5B). This same approach is used for analysing conical folds (e.g., Fernández et al., 2003). By analogy, bedding measurements of a fan-shaped rock body (Fig. 5C) will only be distributed along an arc segment of a small circle (Fig. 5D). This arc represents the intercept of the measured surface with the lower hemisphere of the stereographic diagram, and thus the fan-shaped geometry of an ancient sedimentary unit can be approximately tested. The arc convexity points in the same direction as the fan axis plunge, while the apex is orientated in the opposite direction (Fig. 5E). An estimate of the fan slope angle can be deduced from the diagram as an approximation to the arc's vertical angle measured from the horizontal great circle. This method can also be helpful in determining whether alluvial units constitute single fans or more complex rock bodies, i.e., coalesced fans or bajadas. In any case, the current method cannot be implemented in an isolated way. Its reliability has a strong dependence on the geological context and the results should always be used to complement the analysis of other geological and sedimentary characteristics such as the distribution of bedding dip and strike in the area (map view and cross-section analysis), clast provenance, catchment area lithologies, paleotransport directions and depositional processes. Finally, the current method is compatible with units that have

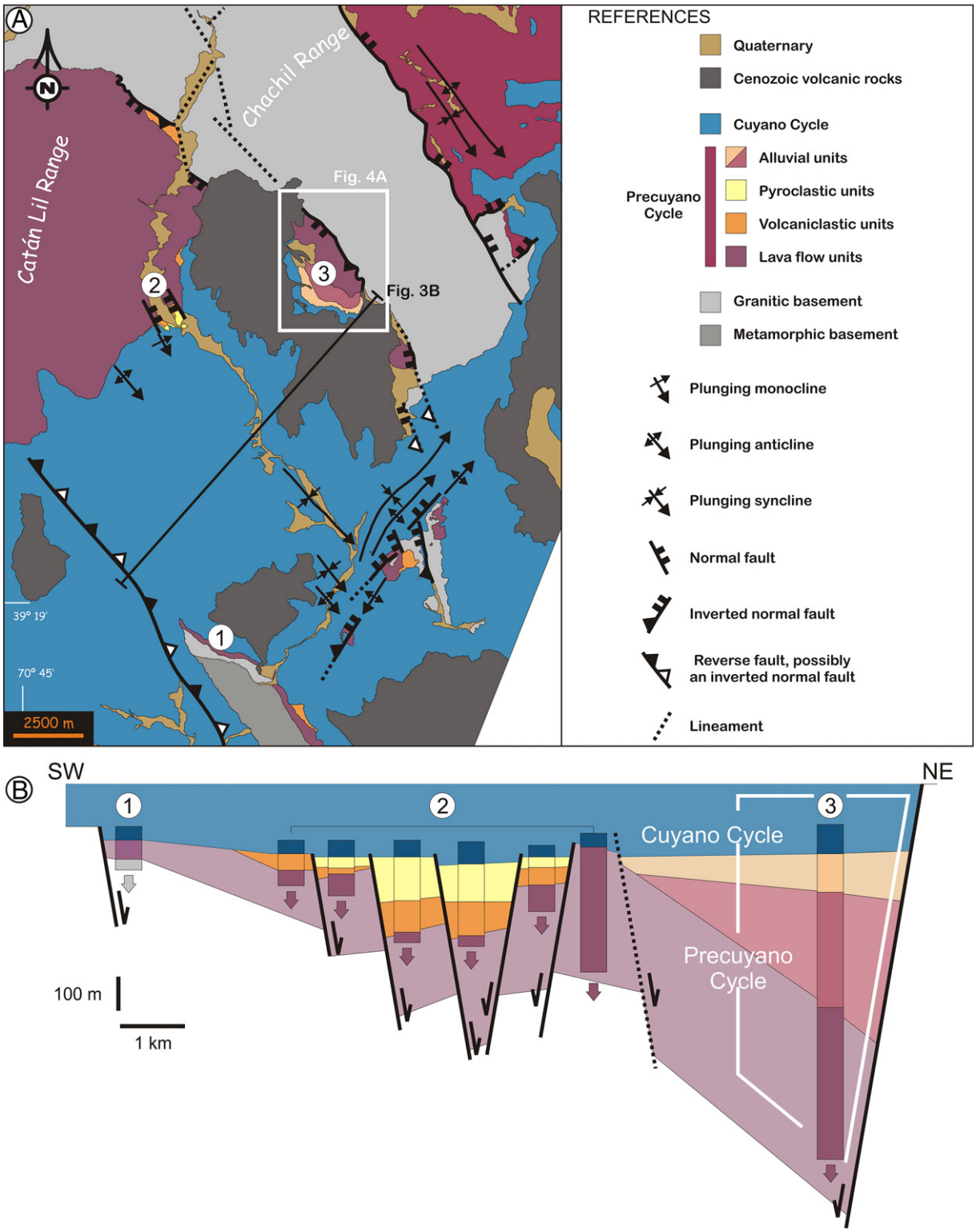

Fig. 3. (A) Map of the Catán Lil Depocentre. (B) Correlation panel and schematic reconstruction of cross section geometry based on the thickness of units at different locations in the depocentre: southwestern border (1), interior (2) and northeastern border (3). Total length of the panel is 13.5 km. Location of the studied alluvial succession is indicated with a white rectangle in map view (A; see Fig. 4A) and with white lines in the correlation panel (B).

suffered rigid body deformation (e.g., tectonic tilt), as they can always be restored to their previous orientation by simple stereographic rotation techniques (e.g., Fernández et al., 2003). However, it should only be conducted when the bedding is not affected by non-rigid body deformation (e.g., folding, faulting, and fluid escape). Clast provenance for each unit was determined in the field by counting clasts along a square matrix of 10 by 10 nodes at each counting site. Spacing between nodes was kept equal to the average clast size in each case. Because of the presence of matrix in Unit 1, counts were done separately for clast and matrix fraction in this case. In order to provide detailed quantification of compositional variations observed in Unit 2, four sample stations were arranged following a vertical trend along Log 4 (Figs. 4, 6). Each station

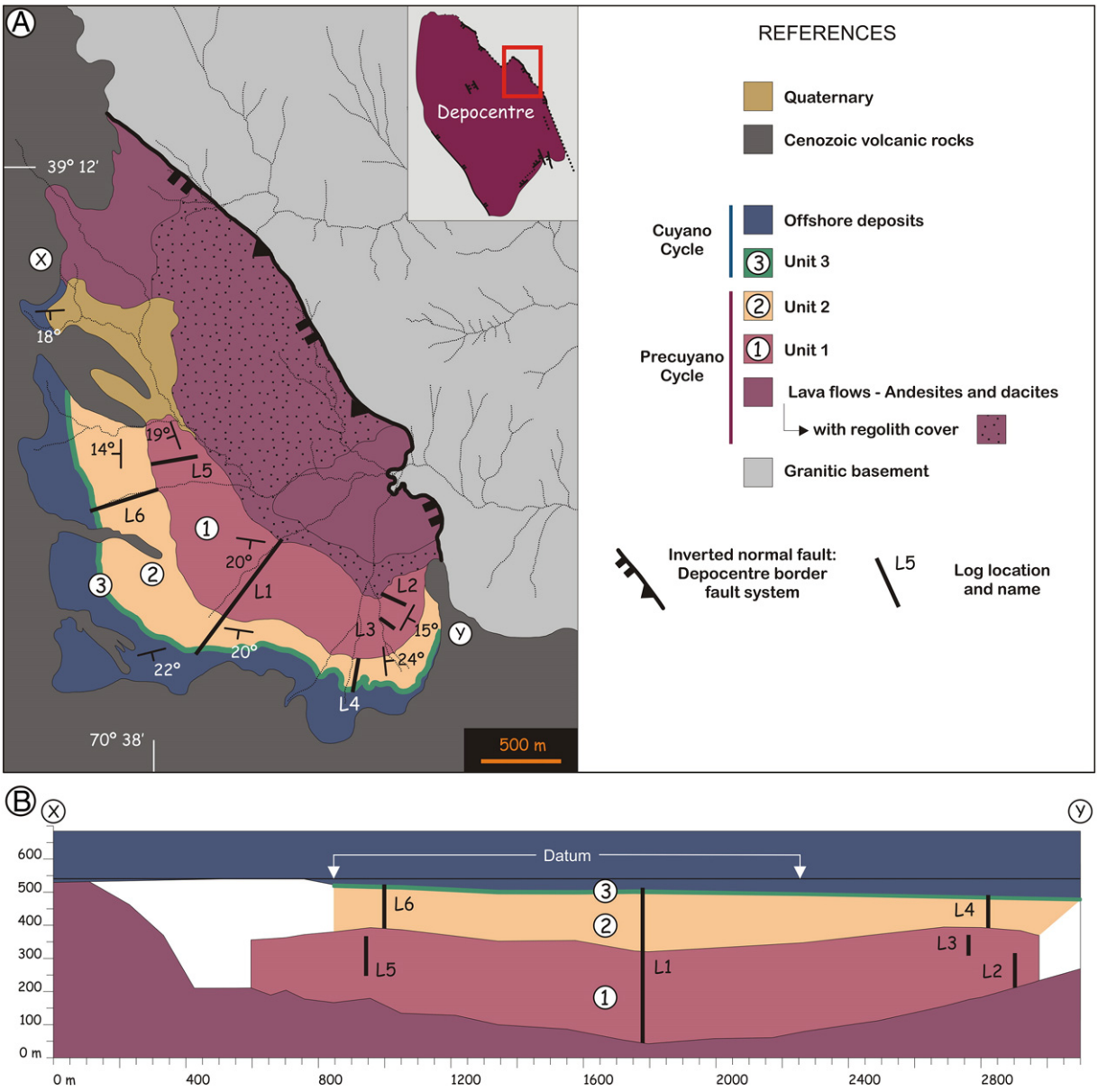

Fig. 4. (A) Map of the study area, including the locations of the sedimentary logs (L1–6). (B) 2D section between map positions X and Y, levelled with offshore deposits internal strata. Sedimentary log relative positions are projected onto this section. Logs are presented in Fig. 6.

included 10 counting sites, adding up a total of approximately 1000 counts per station.

5. Alluvial deposits

Four different facies were defined for Unit 1, two for Unit 2 and two for Unit 3. Their descriptions are given below and summarised in Table 1. Compositional data are shown in Tables 2–4 for Units 1, 2 and 3, respectively.

5.1. Unit 1

Unit 1 constitutes the only evidence of alluvial deposits with basement provenance along the northeastern border fault system (Fig. 3A). It spans from 135 to 273 m thick and is composed mainly of granite-derived coarse-grained conglomerates that unconformably overlie the irregular topography left on top of the lava flow units in the hangingwall (Figs. 4, 6–8). This volcanic substratum shows variable degrees of alteration and regolith formation on its top surface (Fig. 4A), forming a weathering zone up to almost 2 m thick.

5.1.1. Facies 1A

This is the commonest facies present in Unit 1 (Fig. 6). It consists of poorly sorted clast-supported to matrix-supported cobble to boulder conglomerates (Figs. 7A, 8A,B). Clasts are mainly granitic (>80% of the grain fraction). Mean clast-size range is 12 to 30 cm and maximum granitic clast size reaches 60 to 120 cm. Volcanic clasts are smaller, spanning 3 to 10 cm and reaching a maximum of 40 cm. Granitic clasts are rounded while volcanic ones are angular. Matrix fraction is composed of granules with a proportion of 59% granitic and 41% volcanic granules (Table 2). Beds 1–5 m thick are tabular with irregular bases and planar tops. They are commonly massive but sometimes they show coarse-tail inverse grading at the base of the deposits.

Successions constituted by Facies 1A can be solely composed of the above mentioned deposits, but they are also frequently found

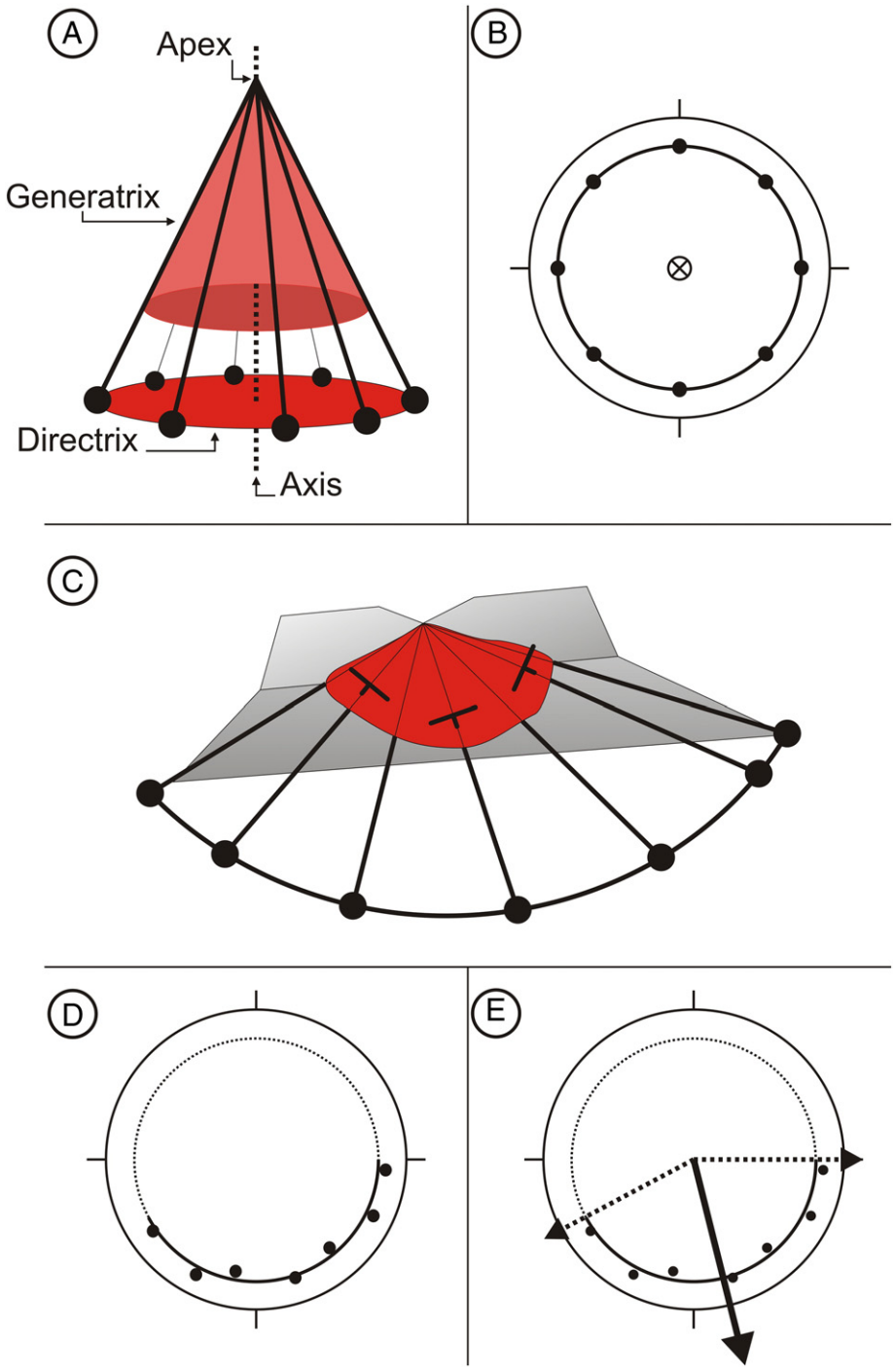

Fig. 5. Geometrical comparison between a cone and an alluvial fan. (A) Perspective view of a vertical cone. The perimeter of the base of a cone is called the directrix, and each of the line segments between the directrix and apex is a generatrix of the lateral surface. (B) The stereographic projection of the generatrices of the cone shown in (A) defines a small circle with the axis projected into its centre. (C) Perspective view of an idealised alluvial fan. The alluvial fan corresponds to a section of a cone: by analogy, measurements of bedding dip and dip direction are equivalent to the generatrices of that same cone section. (D) The stereographic projection of the measurements of bedding dip and dip direction on the alluvial fan (C) distributes along an arc segment of a small circle. (E) Theoretical span of the alluvial fan in (C). The bigger arrow marks the central direction. Ideally, the catchment area would be situated somewhere opposite to where the central arrow is aiming.

intercalated with Facies 1C or Facies 1D deposits (Figs. 7C, 9A,C). Facies 1A successions are not thicker than 12 m.

5.1.2. Facies 1B

This facies is irregularly distributed at the base of Unit 1 and the successions are always less than 15 m thick (Fig. 6, Log 1). It is composed of very poorly sorted matrix-supported boulder conglomerates (Figs. 7B, 8C,D). Clasts are granitic (>90%), subrounded and 60 to 120 cm of maximum size. Matrix is composed of sand and silt of volcanic origin with granitic granules in a proportion similar to that of Facies 1A (Table 2). Beds are tabular, with planar irregular bases and tops and measure 0.5 to 2.5 m thick. Coarse-tail normal and inverse-normal grading is found. Facies 1B is commonly composed of successions of amalgamated beds.

5.1.3. Facies 1C

Facies 1C consists mainly of moderately to well-sorted clast-supported pebble and cobble conglomerates (Figs. 7C, 9A). Grain

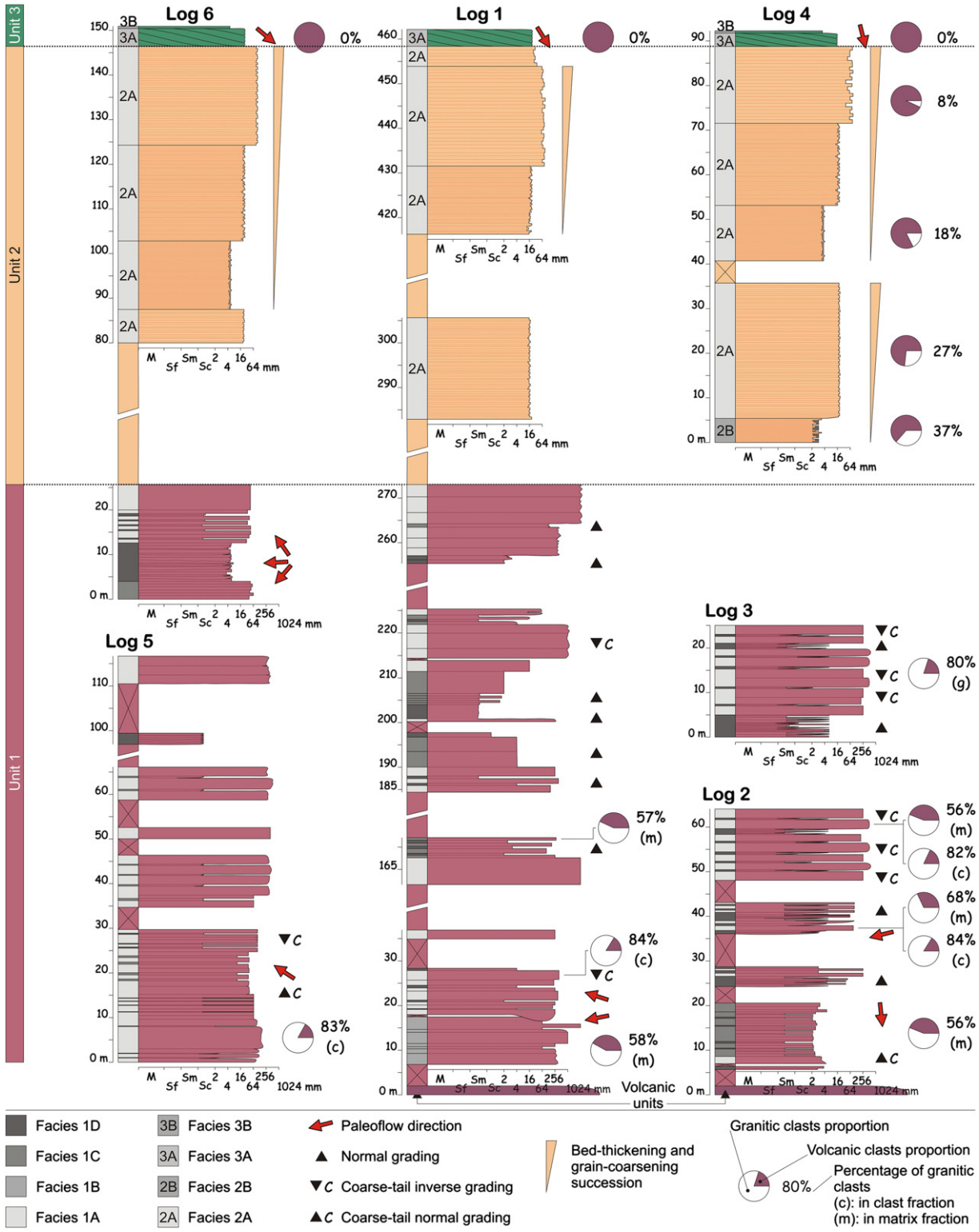

Fig. 6. Schematic sedimentary logs showing facies distribution, grain size, bed thickness and paleoflow directions. See Fig. 4 for log locations. Two coarsening and bed-thickening upwards cycles can be appreciated for Unit 2 in Log 4. The lower one is composed of Facies 2B followed by Facies 2A. The upper cycle is completely composed of Facies 2A. Facies 3A clinoforms downlap on top of Facies 2A successions. Facies 3A is capped by Facies 3B in Log 4 and Log 6. Note the gradual vertical decrease in granite-derived clasts through Unit 2 until their complete disappearance in Unit 3. For further detail on compositional analysis refer to Tables 2–4.

composition is the same as for Facies 1A (Table 2). Clasts are rounded to well-rounded for granite and angular for volcanics. They also include a few outsized clasts 20 to 40 cm long. Less regularly, boulder conglomerates are also found as part of this facies. Tabular and channelized matrix-free bodies are observed with planar or trough cross- or horizontal stratification and rare clast imbrication. They are 30 to 80 cm thick and can extend laterally for up to 3 m. Channel bases are erosive with a step-like configuration, while tops are planar.

Facies 1C is commonly intercalated with Facies 1A constituting 5 to 12 m thick successions. Channel bodies are rarely erosive over Facies

Table 1
Summary of facies main characteristics of the studied alluvial units in the Catán Lil Depocentre.

Facies	Lithology	Structures and geometry	Thickness and width
1A	Poorly sorted clast- to matrix-supported cobble to boulder conglomerates	Massive tabular beds with irregular bases and planar tops	T: 1 to 5 m; W: 10 to 30 m
1B	Very poorly sorted matrix-supported boulder conglomerates	Massive tabular beds with irregular bases and planar tops	T: 0.5 to 2.5 m; W: 5 to 20 m
1C	Moderately to well sorted clast-supported pebble and cobble conglomerates	Tabular beds or lenses with horizontal, planar or trough-cross stratification	T: 0.3 to 0.8 m; W: 1 to 2.5 m
1D	Moderately to well sorted clast-supported granule and pebble conglomerates and well sorted clast-supported sandstones	Tabular beds or lenses massive, diffusely or horizontally stratified	T: 0.2 to 0.35 m; W: 1 to 3 m
2A	Very well sorted clast-supported pebble conglomerates	Massive or diffusely stratified tabular beds with planar bases and tops	T: 0.2 to 0.8 m; W: 2 to 12 m
2B	Very well sorted clast-supported granule conglomerates	Stratified tabular beds with planar bases and tops	T: 0.05 to 0.15 m; W: 2 to 3 m
3A	Very well sorted clast-supported pebble conglomerates	Oblique clinoforms made of massive or diffusely stratified tabular beds	T: 0.3 to 0.8 m; W: up to 15 m; Clinoform height: 2.5 to 5.5 m
3B	Very well sorted clast-supported granule conglomerates (marine bivalves + black shale intraclasts)	Evenly stratified tabular beds with planar bases and tops	T: 1 to 5 m; W: 10 to 30 m

1A and are never deeply incised. However, they commonly erode other Facies 1C deposits (Fig. 9A). Exclusive Facies 1C successions are not frequent and measure up to 9 m thick (Fig. 6).

5.1.4. Facies 1D

Two different kinds of deposits constitute Facies 1D. The first one includes conglomeratic and sandy successions consisting of lenticular and tabular beds. They are composed of moderately well sorted clast-supported granule and pebble conglomerates intercalated with well-sorted sandstones. Lenses are massive to diffusely stratified (Fig. 9C). They show concave bases and planar tops, measure 20 to 30 cm thick, and are normally graded. Tabular bodies are also massive to diffusely stratified, 20 cm thick, and show planar bases and tops (Fig. 9B). The proportion of granitic/volcanic clasts is identical to that in the matrix of Facies 1A (Table 2). Isolated cobble rounded granitic clasts are commonly present. The second type of deposit is composed of well-sorted and clast-supported granule conglomerate lenses. These lenses show horizontal stratification, concave bases and planar tops, and measure 25 to 35 cm thick. They often carry either granitic or volcanic cobble clasts.

Facies 1D commonly appears intercalated with Facies 1A, in 10 to 20 m thick successions (Fig. 7A). Exclusive Facies 1D successions are less than 8 m thick and are sparsely and irregularly distributed throughout Unit 1 (Fig. 6).

5.1.5. Unit 1 sedimentary processes

The poorly sorted cobble to boulder conglomerates which make up Facies 1A and 1B are characteristic of debris flow deposition (e.g., Smith, 1986; Blair and McPherson, 1992, 1994, 1998; Blair, 1999b). The major difference between these facies lies in clast concentration and matrix grain-size. Facies 1A has a granule-size matrix while it is finer for the volcanic components of Facies 1B matrix. This can be attributed to differences in flow cohesive rheology. The nature of the matrix particles is a key factor in grain support mechanisms within debris flows (Blair and McPherson, 1992, 1994, 1998; Dasgupta, 2003). Clay content proportion determines the cohesive or non-cohesive character of the flow (>27% cf., Dasgupta, 2003, and discussion therein; Wagreich and Strauss, 2005). Clay was observed neither in Facies 1A nor in Facies 1B. The lack of any distinguishable cohesive particles in Facies 1A indicates its deposition by non-cohesive flows. The poorer sorting and lower clast concentration observed in Facies 1B cannot be taken unequivocally as a proof of cohesiveness. Nevertheless, they do suggest a more cohesive nature for the debris flows represented by Facies 1B than for those represented by Facies 1A.

Facies 1C and 1D are clearly better sorted than Facies 1A and 1B. The structures developed in Facies 1C such as planar and trough cross-stratification, in addition to the better development of horizontal stratification, imply turbulent current conditions. Channel bodies are well defined and show relatively complex erosive features whose form in cross section resemble channel fills preserved between Facies 1A debris flow deposits. Facies 1C is the result of secondary fluidal flow processes occurring between events of debris flow deposition (Blair and McPherson, 1992, 1994, 1998; Blair, 1999b). The fact that the channels are only rarely found incised into the debris flow deposits suggests the superficial reworking character of the involved processes. Successions exclusively composed of Facies 1C represent more persistent fluidal deposition conditions in localised positions along Unit 1. They may be related to the existence of incised channels (e.g., Blair, 1999b) but none of these could be readily distinguished in the outcrops. Facies 1D clast-size is finer than that of Facies 1C; it lacks any conclusive evidence of turbulent deposition, and also presents channel-like bodies, albeit of a much smaller scale. These lenses do not show erosive bases. The arrangement of massive tabular beds and normal graded lenses can be explained by rapid water-flow deposition by flashy flood surges (e.g., Blair and McPherson, 1994). These types of flows can range from truly fluidal to even hyperconcentrated. Facies 1D was originated under less

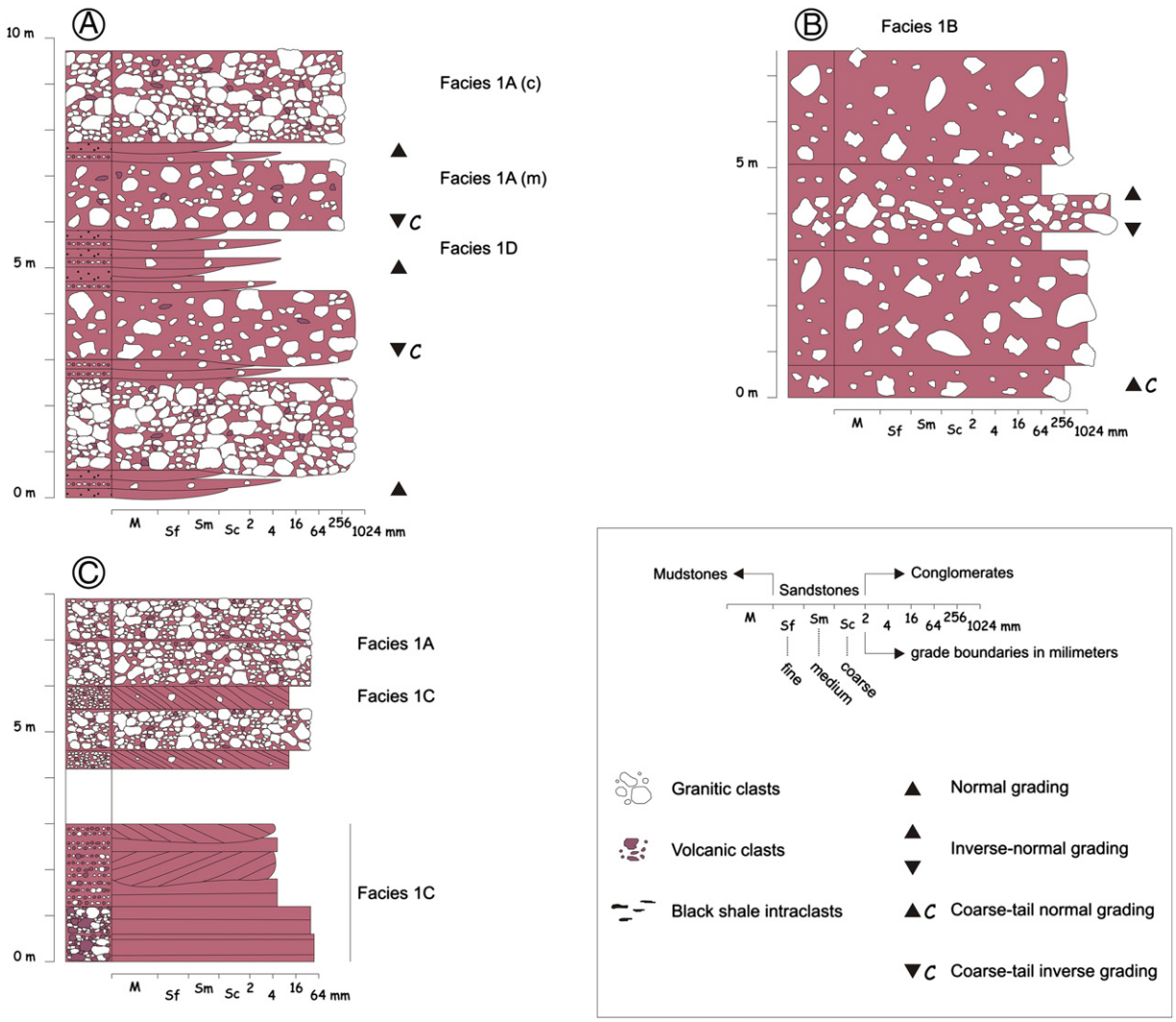

Fig. 7. Typical log sections for Facies 1 deposits. (A) Facies 1A succession with intercalations of Facies 1D deposits; clast-supported Facies 1A deposits indicated as (c) and matrix-supported ones as (m). (B) Facies 1B succession. (C) Facies 1C at the base of the log section, followed by intercalations between Facies 1C and Facies 1A. (A), (B) and (C) correspond to actual sections from Logs 3, 1 and 5, respectively (See Fig. 6). Keys are indicated inside the box.

energetic conditions than Facies 1C but the two are equivalent in terms of being deposited in between major debris flow event deposits (Blair and McPherson, 1992, 1994, 1998; Blair, 1999b).

The difference between volcanic- and granitic-derived clasts is not only compositional but also in terms of shape and size. Granitic clasts are rounded to subrounded while volcanic ones are invariably angular. The proportion of granitic clasts in Unit 1 is higher in the coarser-grained beds and it decreases in the finer-grained deposits and the matrix fraction (Table 2). Overall abundance of granitic clasts reflects the predominance of this lithology in the bedrock catchment area, which is indicative of a footwall block derived provenance (Fig. 4). This special signature is evidently weaker in the finer portions because of the contribution of fragments derived from weathering of the volcanic substratum. Volcanic clasts were thus incorporated to the different flows in the hangingwall area after the flows left the footwall catchment zone. The lower proportion of coarser volcanic clasts is explained by the implied lower gradient in the hangingwall area.

5.2. Unit 2

Unit 2 unconformably overlies Unit 1 along a sharp and abrupt contact (Fig. 4). It is a 92 to 128 m thick succession composed of volcanic-derived medium- to fine-grained conglomerates. This compositional trend becomes more marked upwards throughout the unit (Table 3; Fig. 6, Log 4). Almost the entire unit is formed by Facies 2A (Figs. 6, 10, 11).

5.2.1. Facies 2A

Facies 2A comprises very well sorted clast-supported mixed provenance pebble conglomerates, with an absence of matrix (Figs. 10A, 11A). Volcanic clasts are characteristically angular to subangular in shape while granitic ones tend to be rounded. Average clast-size ranges from 4 to 64 mm, with granitic clasts generally smaller than volcanic ones. However, isolated outsized rounded granitic and volcanic cobbles and boulders are present, measuring 40 to 120 cm (Fig. 11B). The successions are conspicuously composed of 20 to 80 cm thick massive to diffusely stratified tabular beds, with planar bases and tops (Fig. 11B). Less frequently, couplets 30 to 50 cm thick, of pebbly (15 to 30 cm thick) and granule (5 to 20 cm thick) conglomerates, are observed (Fig. 11C). Facies 2A successions are 80 to 180 m thick and are typically coarsening- and bed-thickening upwards (Figs. 6, 11D). Large volcanic-derived blocks are commonly found near the top of Unit 2 (Fig. 11E).

5.2.2. Facies 2B

Very restrictedly, it occurs only at the base of Unit 2 (Fig. 6, Log 4) and it is mainly differentiated from Facies 2A by its finer grain-size. It is composed of very well sorted clast-supported granule conglomerates (Figs. 10B, 11F). There is no matrix in these deposits. Volcanic clasts are

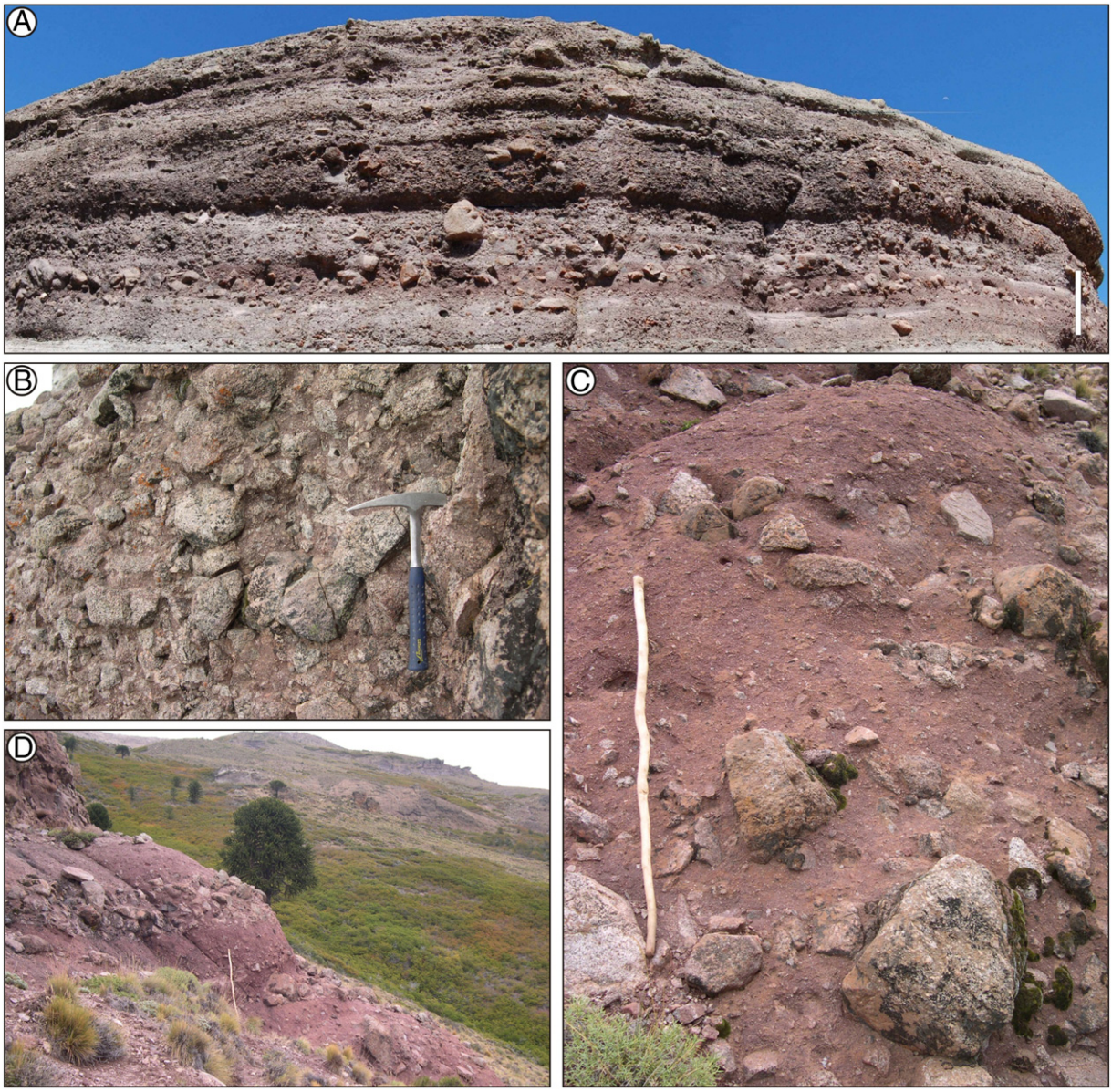

Fig. 8. Field photographs of the conglomerate deposits in Unit 1. (A) Succession of stacked tabular beds of poorly sorted conglomerates (Facies 1A). (B) Clast rich conglomerates (Facies 1A). (C) Very poorly sorted matrix-supported boulder conglomerate (Facies 1B). (D) Succession of amalgamated beds of matrix rich conglomerates (Facies 1B). Wooden stick and white bar for scale are 1.2 m, hammer is 30 cm long.

subangular, while granitic ones are rounded to subrounded. Clast-size ranges from 2 to 4 mm, with rare volcanic fragments measuring 4 cm and definitely outsized rounded granitic boulders of up to 60 cm. Beds are stratified, showing tabular geometry with planar bases and tops, 5 to 15 cm thick. Successions composed by Facies 2B tend to be about 5 m thick.

5.2.3. Unit 2 sedimentary processes

Well-sorted clasts, the lack of matrix fraction and the occurrence of massive to diffusely stratified beds in Facies 2A suggest hyperconcentrated flow deposition (Smith, 1986; Blair and McPherson, 1994; Blair, 1999a,c) while the better stratified Facies 2B may correspond to deposition from more diluted flows. The only other difference is the coarser nature of Facies 2A, implying higher energy conditions for this facies. These features, along with the couplet grain-size alternations, are typical characteristics of sheet-flood dominated alluvial systems (Blair and McPherson, 1994; Blair, 1999a,c). Outsized clasts are indicative of the competence of the sheetfloods (e.g., Blair, 1999a). However, it is also possible that some of them were transported by rolling from nearby heights. Neither Facies 2A nor 2B present any clear evidence of erosive processes within Unit 2 deposits. Predominance of volcanic over granitic clasts (Table 3) implies a catchment area dominated by volcanic bedrock, suggesting a catchment situated mostly in the hangingwall (Fig. 4). Facies 2A contains footwall-derived (granitic) as well as hangingwall-derived (volcanic) boulders. On the contrary, Facies 2B contains only footwall-derived boulders.

5.3. Unit 3

Unit 3 is only 3 to 6 m thick. It is composed of medium- to fine-grained conglomerates that always overlie Unit 2 deposits, separated by an irregular but not incised erosion surface (Fig. 6), and are covered by black shales (Fig. 4). Almost all of Unit 3 is composed by Facies 3A and its composition is characteristically volcanic-derived (Table 4).

5.3.1. Facies 3A

Facies 3A comprises very well sorted clast-supported matrix-free pebble conglomerates (Fig. 10C). Clasts are angular to subangular and

Table 2
Unit 1 compositional data. See Fig. 4 for log locations and Fig. 6 for station positions along logs.

Location	L2	L2	L1	L2	L1	Total	Total (%)
Latitude (S)	39°13′31″	39°13′32″	39°13′14.8″	39°13′25.5″	39°13′31.2″		
Longitude (W)	70°36′59″	70°36′58.2″	70°37′34.2″	70°37′35.2″	70°37′1.7″		
Facies	1A matrix	1A matrix	1B matrix	1C clasts	1C clasts		
	Station 1	Station 2	Station 3	Station 4	Station 5		
Granitic clasts	56	68	58	55	58	295	59
Volcanic clasts	44	32	42	43	44	205	41
n	100	100	100	98	102	500	
Location	L2	L2	L3	L1	L5	Total	Total (%)
Latitude (S)	39°13′31″	39°13′32″	39°13′34.6″	39°13′15.8″	39°12′47.3″		
Longitude (W)	70°36′59″	70°36′58.2″	70°37′1.4″	70°37′33″	70°38′5.1″		
Facies	1A clasts	1A clasts	1A clasts	1A clasts	1A clasts		
	Station 1	Station 2	Station 6	Station 7	Station 8		
Granitic clasts	82	84	80	84	83	413	83
Volcanic clasts	18	16	19	16	17	86	17
n	100	100	99	100	100	499	

totally of volcanic provenance (Table 4). Average clast-size is 12 to 15 mm, reaching a maximum of 7 cm. Some fragmented and disarticulated marine bivalves are also present. The most conspicuous feature of this facies is the development of oblique clinoforms with an average dip of 19° and up to 15 m long (Fig. 12). Clinoforms height varies from 2.5 m at the southeast (Fig. 4A,B, between Logs 4 and Y) to 4 m at the northwest (Fig. 4A,B, Log 6), locally reaching up to 5.5 m to the north of Log 6 (Fig. 4A,B). The clinothems are massive to diffusely stratified tabular beds with net planar bases and tops and are 30 to 80 cm thick (Fig. 12). They downlap onto Facies 2A deposits and are developed throughout Facies 3A successions (Fig. 6). No outsized clasts were observed in these deposits.

5.3.2. Facies 3B

Facies 3B is only present in some locations and always overlies Facies 3A (Figs. 6, 10C). It includes evenly stratified and very well sorted clast-supported granule conglomerates. While clasts are mainly volcanic, marine bivalve fragments are also present. Less common are platy black shale intraclasts which are aligned parallel to stratification. This facies is only 50 cm thick.

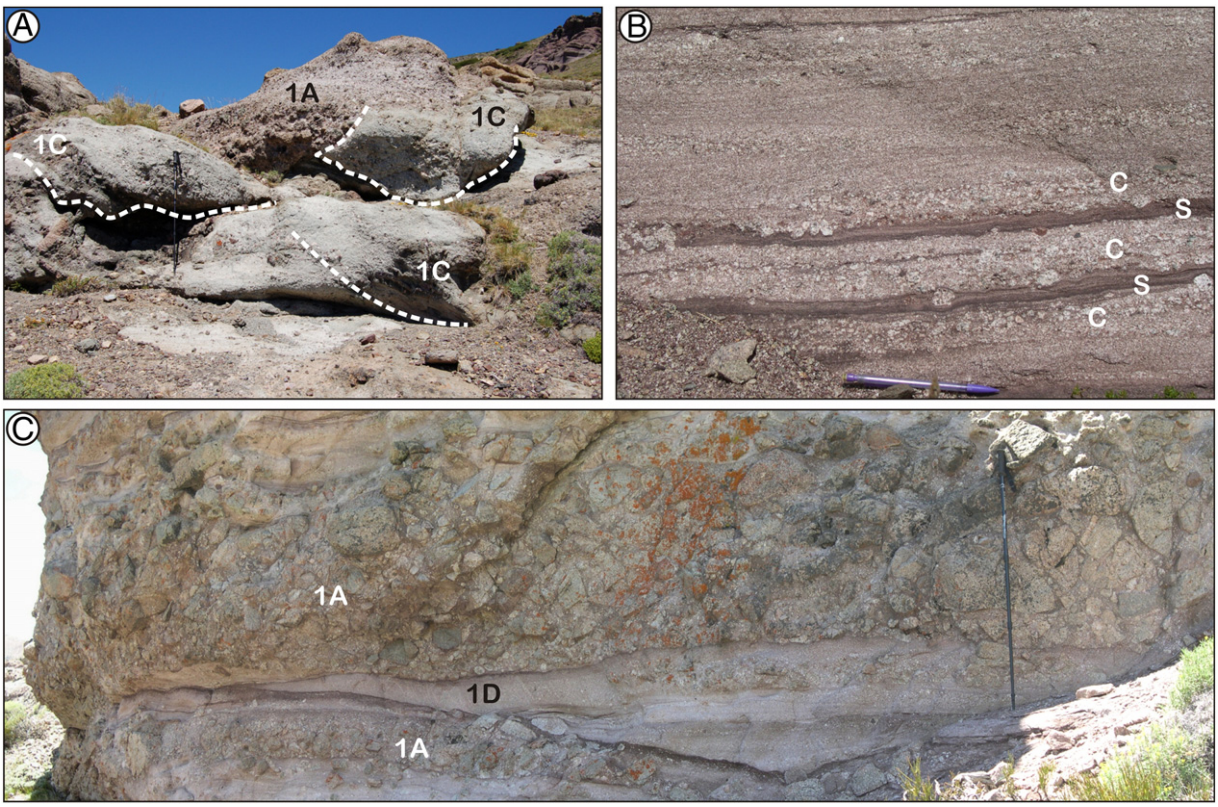

Fig. 9. Field photographs of the conglomerate deposits in Unit 1 (A) Channelized well sorted conglomerates (Facies 1C). (B) Well sorted sandstones (S) intercalated with moderately well sorted fine conglomerate (C) deposits (Facies 1D). (C) Gully fill composed of moderately well sorted coarse sandstones and fine conglomerates (Facies 1D) in between two coarser-grained conglomerate deposits (Facies 1A). Trekking pole for scale is 1.2 m long and pencil is 7 cm long.

Table 3
Unit 2 compositional data. See Fig. 4 for log locations and Fig. 6 for station positions along L4. CS, counting site.

	CS 1	CS 2	CS 3	CS 4	CS 5	CS 6	CS 7	CS 8	CS 9	CS 10	Total	Total (%)
L4 — station 9 (lower section): Facies 2B. Coordinates: 39°13′43.3″S, 70°37′6.7″W												
Granitic clasts	30	48	44	37	43	28	36	36	35	39	376	36.90
Volcanic clasts	71	52	66	62	57	82	64	64	64	61	643	63.10
n	101	100	110	99	100	110	100	100	99	100	1019	
L4 — station 10 (lower middle section): Facies 2A. Coordinates: 39°13′44.1″S, 70°37′6″W												
Granitic clasts	29	34	24	36	28	23	26	29	23	29	281	27.41
Volcanic clasts	71	75	76	74	77	77	74	71	78	71	744	72.59
n	100	109	100	110	105	100	100	100	101	100	1025	
L4 — station 11 (upper middle section): Facies 2A. Coordinates: 39°13′44.8″S, 70°37′5.8″W												
Granitic clasts	23	23	18	15	22	15	24	18	15	12	185	18.52
Volcanic clasts	77	77	82	85	78	85	76	82	85	87	814	81.48
n	100	100	100	100	100	100	100	100	100	99	999	
L4 — station 12 (upper section): Facies 2A. Coordinates: 39°13′45.9″S, 70°37′7″W												
Granitic clasts	8	5	9	9	10	6	7	7	6	12	79	7.85
Volcanic clasts	92	95	91	91	90	94	93	93	94	94	927	92.15
n	100	100	100	100	100	100	100	100	100	106	1006	

5.3.3. Unit 3 sedimentary processes

There is a great resemblance between Facies 2A and Facies 3A, revealed in grain size, clast composition (Table 4) and shape, well sorted condition and complete lack of a matrix fraction. Geometry and structure of the beds are also very similar. Facies 3A is thus also interpreted to represent deposition from hyperconcentrated flows (Smith, 1986; Blair and McPherson, 1994; Blair, 1999a,c). Nevertheless, the conspicuous development of well defined clinoforms throughout the deposits is an unequivocal evidence of subaqueous deposition and typical of deltas (e.g., Postma, 1990; Orton and Reading, 1993). As clinoform height approximately represents the paleo-bathymetry during deposition (e.g., Postma, 1990; Mortimer et al., 2005) it would imply in this case a depth of water between 2.5 and 5.5 m, which is typical of shoal-water deltas (Postma, 1990). The facies are characteristically very similar between the subaerial and subaqueous parts of this type of deltas (Postma, 1990; Orton and Reading, 1993). The oblique geometry of the clinoforms indicates a dominance of progradation over aggradation in the depositional system (e.g., Mortimer et al., 2005). The thin, but widespread occurring Unit 3 deposits, together with the implied shallow water, are compatible with that progradational scenario. The presence of the bivalve fragments in Facies 3A argues for marine conditions in the depositional environment. In this sense, Facies 3A represents the continuation of hyperconcentrated flow deposition resulting from a sheet-flood dominated alluvial system (Blair and McPherson, 1994; Blair, 1999a,c) that projected into the marine realm in a fan delta setting (McPherson et al., 1987; Sohn and Son, 2004; Blair and McPherson, 2008).

Facies 3B is the product of less energetic and more diluted flows at the end of Unit 3 deposition. Facies 3B thin and discontinuous in nature together with its content of broken shells and clay intraclasts are characteristics referable to transgressive lags (e.g., Cattaneo and Steel, 2003). Their occurrence on top of Facies 3A foresets could represent the transgression that led to the deposition of the black shale units that overlie Unit 3.

An overall gradual decrease in the clinoform height is noted for most of the exposure from 4 to 2.5 m (Fig. 4A,B, between Logs 6 and Y). The fact that this decrease coincides with the progradation direction could indicate a relative fall in sea level (~1.5 m) before the transgression that deposited Facies 3B and the subsequent black shales occurred. The combined effect of sea level fall followed by a transgression, and its consequent erosional effect, could account for the lack of preserved clinoform tops in Unit 3. Caution is needed interpreting any relative sea level fall from the preserved height of the clinoforms as it is possible that some of the observed variations respond to local irregularities inherent to the inundating nearshore substrate (i.e., top of Unit 2). Also, only a sharp non-incised surface is observed between Facies 3A and Facies 3B (Figs. 6, 10C). Facies 3B grain-size is significantly smaller than Facies 3A (Figs. 6, 10C), so if similar grain-sizes are assumed between topset and foreset, Facies 3B does not possibly represent reworking of any Unit 3 clinoform tops.

Except for the bivalve fragments and the black shale intraclasts, all the other clasts forming Facies 3 are volcanic. This is compatible only with a catchment area entirely placed on the hangingwall block.

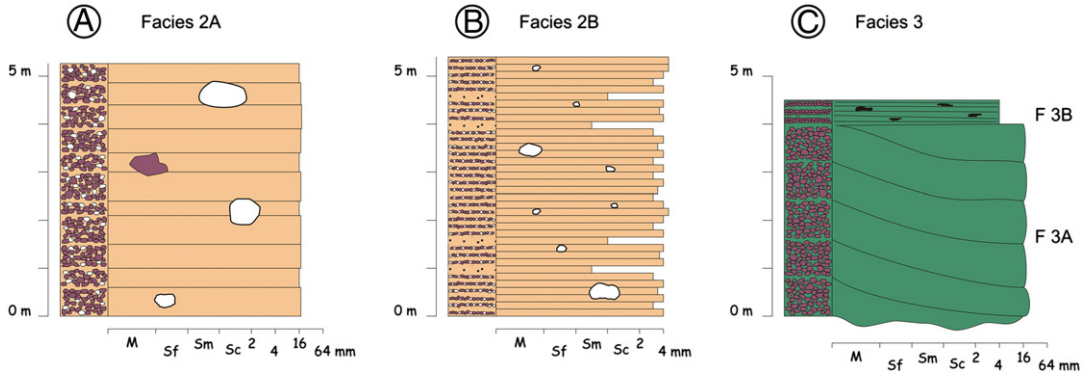

Fig. 10. Typical log sections for Facies 2 and 3 deposits. (A) Facies 2A. (B) Facies 2B. (C) Facies 3; Facies 3A and 3B indicated as F 3A and F 3B, respectively. (A), (B) and (C) correspond to actual sections from Logs 1, 4 and 6, respectively (See Fig. 6). See Fig. 7 for keys.

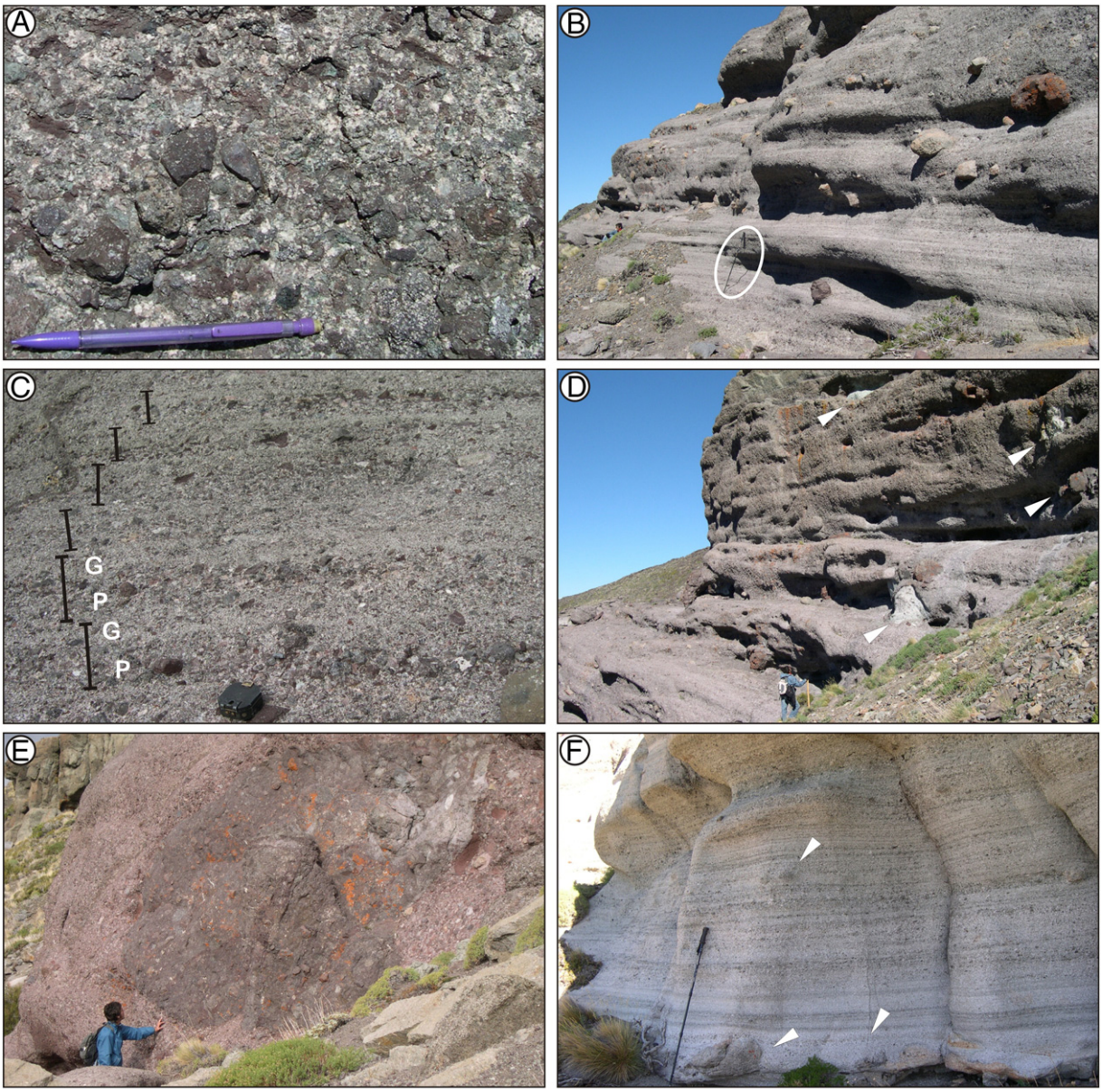

Fig. 11. Field photographs of the conglomerate deposits in Unit 2. (A) Typical deposit composed of well sorted conglomerates (Facies 2A) with angular volcanic clasts; pencil for scale is 15 cm long. (B) View of Unit 2 lower middle section. Tabular stratified beds with dispersed outsized boulders (Facies 2A); trekking pole (circled) for scale is 1.2 m. (C) Couplet alternation between pebble (P) and granule (G) conglomerates (Facies 2A); compass for scale is 7 cm wide. (D) View of Unit 2 upper section. The succession is bed-thickening and grain-coarsening upwards; compare with (B). The outsized boulders get even bigger (some arrow marked); see person for scale. (E) Outsized volcanic derived block of about 5 m long and 3.2 m across; see person for scale. (F) View of Unit 2 base. Tabular well stratified beds made of granule conglomerates (Facies 2B) with outsized cobbles and boulders (some arrow marked); trekking pole (circled) for scale is 1.2 m.

6. Alluvial evolution

6.1. Composition of the alluvial units

As a whole, the alluvial successions studied show a definite upwards decrease in the proportion of granitic clasts (Fig. 6, Tables 2–4). The change in composition is abrupt from Unit 1 to Unit 2 and is then gradual up to Unit 3. This indicates a general decrease in footwall-derived components and corresponding enrichment in hangingwall-derived ones. It is significant, however, that such diminution is not detected in the case of outsized clasts (i.e., cobbles and boulders), where the relative proportions of granitic and volcanic material do not vary substantially. Unfortunately, the wide dispersion of these fragments prevents obtaining any quantitative result. The presence of scattered granitic cobbles and boulders throughout the thickness of Unit 2 is indicative of a steep gradient in the granitic footwall, where the fault scarp still constituted a positive element shedding occasional debris into the hangingwall during deposition of Unit 2. In contrast, the absence of both volcanic and granite outsized clasts from Unit 3 deposits may imply that locally steep gradients no longer existed either in the hangingwall or the footwall.

Of the two main transport processes detected, each one corresponds to a definite composition: granite-rich units are mainly a product of non-cohesive debris flows while volcanic-rich ones are related to hyperconcentrated flow deposition. No relation of cause and effect is necessarily implied for this particular example, but bedrock lithology has proved in other cases to be a decisive control defining the nature of the flows (Blair, 1999a, 1999b, 1999c; Nichols and Thompson, 2005; Wagreich and Strauss, 2005).

Table 4
Unit 3 compositional data. See Fig. 4 for log locations and Fig. 6 for station positions along logs.

Location	L1	L4	L6	Total	Total (%)
Latitude (S)	39°13′38.7″	39°13′46.8″	39°13′6.1″		
Longitude (W)	70°37′38.4″	70°37′7.4″	70°38′12.9″		
Facies	3A	3A	3A		
	Station 13	Station 14	Station 15		
Granitic clasts	0	0	0	0	0
Volcanic clasts	100	100	100	300	100
n	100	100	100	300	

6.2. Geometry and orientation of the alluvial units

Detailed mapping and surveying of bedding dip and strike of the studied alluvial units do not suggest the existence of coalesced alluvial fans among their deposits (Fig. 4A). On the contrary, the bedding pattern in each unit is more compatible with the one expected for a single fan. The 3D geometry of the alluvial units was evaluated by testing their approximation to a fan shaped body (see Section 4). The results are presented in Fig. 13, along with rose diagrams for the available paleoflow data. In cross-section parallel to the border fault, Unit 1 appears as a lobe deposited over an irregular volcanic surface, depressed in its medial sector (Fig. 13D). Thickness pattern is consistent with this volcanic topography, thickening towards the centre (273 m) and tapering towards the southeast (135 m) and northwest (145 m). No normal faults or synclines are observed affecting the lava flow units below this depression or anywhere else in the study area (Figs. 4, 13). The origin of this depression on top of the lava flow units is thus interpreted to be intrinsic to the volcanic topography. On the other hand, Unit 2 shows moderate wedge geometry with a flatter top gradually sloping to the southeast. Thickness decreases in the same direction from 128 m to the northwest to 92 m to the southeast (Fig. 13D). Unit 3 is a thin wedge-veneer on top of Unit 2, reaching 6 m thick to the northwest and only 3 m thick to the southeast (Fig. 13D).

The distribution of bedding dips (Fig. 13C) and paleoflow directions (Fig. 13B) suggests that the axis of Unit 1 fan was orientated to the southwest, transverse to the border fault system. These data strongly

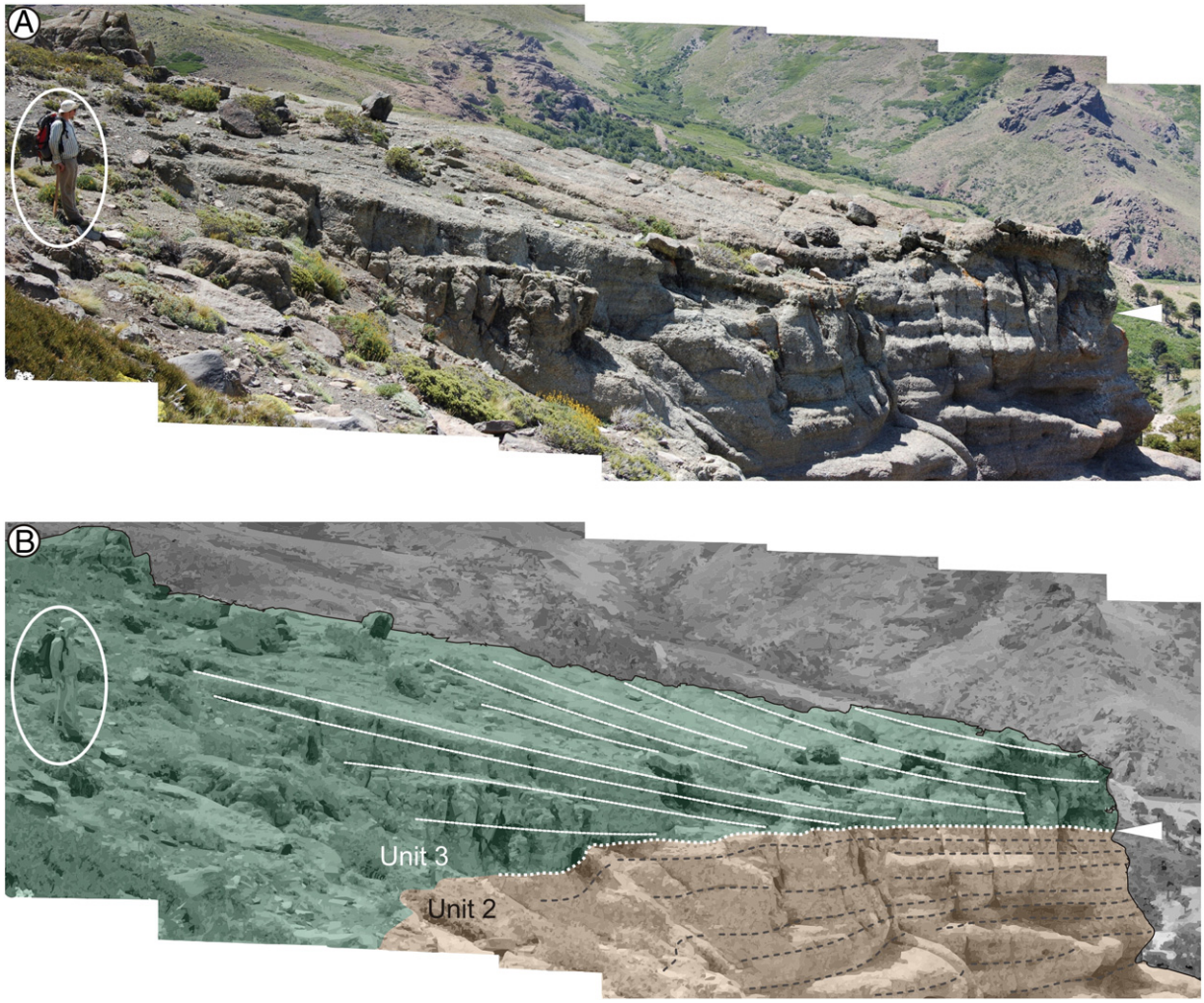

Fig. 12. (A) Typical oblique clinoforms in Unit 3 downlapping directly over Facies 2A deposits from Unit 2. (B) Line drawing and interpretation of (A). Contact between Units 2 and 3 is indicated with a white triangle in (A) and (B) and the trace is highlighted with a white dashed line in (B). Person (circled) for scale is about 1.8 m.

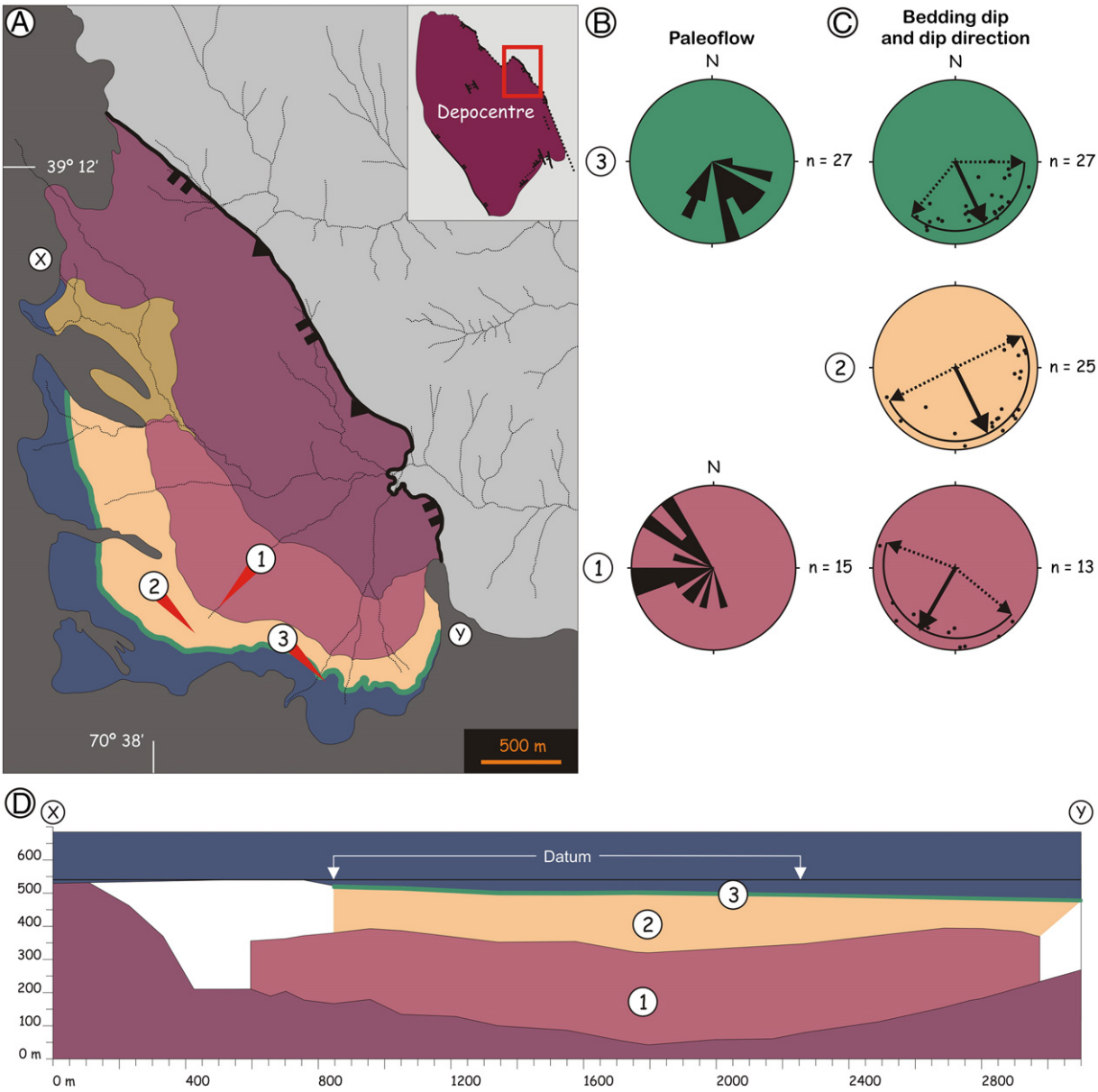

Fig. 13. Analysis of the transport directions for the sedimentary systems represented by Units 1, 2 and 3 deposits and its relation with the depocentre border fault system: Geological map (A) and cross section X–Y (D) of the study area. See Fig. 4. for keys and further explanation. Paleotransport directions are shown for each unit with red triangles in the map (A). (B) Rose diagrams showing paleoflow directions for Unit 1 (cross-stratification, base of channels and clast imbrication) and Unit 3 (foreset clinoforms orientation). (C) Stereographic projections of bedding dip and dip directions for Units 1, 2 and 3. Unit 1 transport direction is to the southwest, transverse to the border fault system. Units 2 and 3 transport direction is to the southeast, parallel to the border fault system.

support Unit 1 being an alluvial fan sourced from the footwall off the northwest–southeast trending border fault. This configuration is consistent with compositional data suggesting a granitic source and the observed cross-sectional lobe geometry (Fig. 13D). In contrast, Unit 2 fan shows an axis orientated to the southeast, parallel to the border fault system, with a fan apex towards the northwest (Fig. 13C). Due to the nature of Unit 2 deposits no paleoflow data can be recorded. However, transport direction expected from the fan configuration for this sedimentary system is from northwest to southeast. Thus, the condition of a hangingwall-fed alluvial system implied by the predominance of volcanic clasts agrees with this fan orientation and the southeastward-tapering wedge geometry observed in the 2D section (Fig. 13D). In the case of Unit 3, the fan delta also shows an axis orientated parallel to the border fault system and a northwesterly pointing apex (Fig. 13C). Transport direction is from northwest to southeast (Fig. 13B), the same direction in which the deposits taper (Fig. 13D).

7. Discussion

Alluvial deposition along the border fault system in a half-graben depocentre is characterised by the development of three distinctive elements (e.g., Leeder and Gawthorpe, 1987; Jackson and Leeder, 1994; Eliet and Gawthorpe, 1995; Leeder et al., 1996; Gawthorpe and Leeder, 2000): a) relatively high-gradient transverse footwall-sourced alluvial fans, b) lower gradient transverse hangingwall-fed alluvial fans typically coalesced into a bajada, and c) an axial river. From these, neither the transverse hangingwall-fed bajada nor the axial fluvial system was found preserved in the current depocentre. Instead, two basic alluvial fan configurations were identified: a footwall-fed fan orientated transversely to the border fault system (Fig. 14A) and a hangingwall-fed fan orientated parallel to the border fault system (Fig. 14B). The first configuration corresponds to Unit 1 and the second to Units 2 and 3.

7.1. Ground tilting and alluvial fan orientation

Hangingwall block rotation determines the topography in the hangingwall surface by ground tilting, controlling the orientation of the alluvial systems in a half-graben (Alexander and Leeder, 1987, 1990; Peakall et al., 2000). It is important to note however, that large footwall-derived sedimentary systems can eventually prograde against the tilt of the hangingwall towards the opposite half-graben margin (e.g., Alexander and Leeder, 1987; Eliet and Gawthorpe, 1995; Leeder et al., 1996). Such a situation only occurs when sedimentation outpaces the creation of accommodation space, which often implies small displacements at the border fault system and consequently low gradients on the hangingwall block (e.g., Alexander and Leeder, 1987; Gordon and Heller, 1993; Eliet and Gawthorpe, 1995; Leeder et al., 1996). This does not apply to the present case as Unit 1 alluvial fan characteristics are related to those of small frontal catchments (sensu Cowie et al., 2006; see Section 7.3, below). Thus, the change in orientation from Unit 1 to Units 2 and 3 can be interpreted to indicate a change in the hangingwall surface gradients. The transverse orientation of the Unit 1 fan can be explained in two possible ways: either its catchment output was situated straight on a topographic low or there were no significant slope gradients along the strike of the border fault system. In any case, it shows that hangingwall block rotation was uniform along strike (Figs. 14C, 15A). The opposite is interpreted to be the case of the longitudinal fan recorded for Unit 2 (Figs. 14D, 15B). The southeastward orientation of this fan consequently needs the existence of a southeastward slope gradient to be explained. Such a change in the hangingwall slope gradients is interpreted to be induced by a southeastward rotation component. Unit 3 fan delta poses a different case. It is difficult to state from Unit 3 data alone whether the hangingwall block experienced any rotation towards the southeast during deposition of the fan delta. Only the gradient of Unit 3 substrate can be inferred. The small and relatively uniform height of clinoforms indicates nearly constant shallow water conditions throughout most of the deposition of Unit 3, suggesting that the substrate for Unit 3 deposition (i.e., top of Unit 2 alluvial fan) was nearly horizontal. The marine transgression represented by the boundary surface between Units 2 and 3 is a regional flooding surface recognised at the base of the Cuyano Cycle. Its effects are widespread all over the Neuquén Basin and a eustatic origin for this transgression is widely accepted (e.g., Gulisano, 1981; Gulisano and Pando, 1981; Legarreta and Uliana, 1996). It is thus proposed that Unit 3 fan delta represents the flooding of the Unit 2 alluvial system, which constituted at that time a low-gradient alluvial fan (Fig. 15C). It is inferred, however, that subsequent pulses of southeast rotation occurred after deposition of Unit 2. While the difficulties to state the case for Unit 3 were exposed above, the wedge geometry of Cuyano Cycle offshore deposits preserved below the beds used as datum for the cross section presented in Figs. 4B and 13D indicates a tilting event towards the southeast after the deposition of Unit 3.

7.2. Possible structural controls on sedimentary patterns

Rotation of the faulted blocks that integrate the hangingwall area is a necessary consequence of the deformation of the highly competent rock units that compose the deforming substrate (granitoids and consolidated lava flow units). Geometrical linkage of fault segments in a normal fault array does not necessarily imply that they behave as a single fault kinematically, and differences in displacement along strike

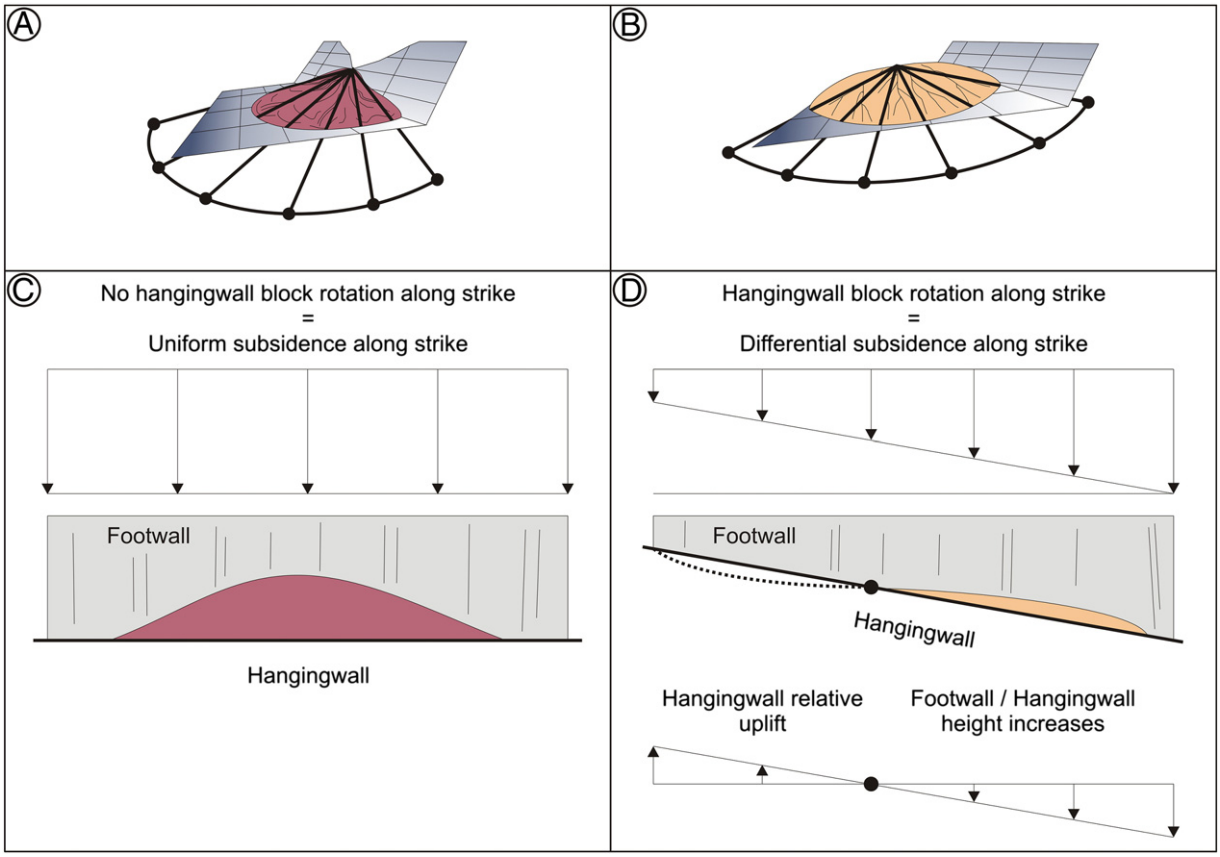

Fig. 14. Schematic diagrams of the alluvial units and their orientation with respect to the depocentre border fault system. (A) Alluvial fan orientated transversely to the border fault system. (B) Alluvial fan orientated parallel to the border fault system. Dip and dip directions shown in (A) and (B). Hangingwall cross-sections, parallel to the border fault system, for a hangingwall block that experiences no rotation along strike (C) and a hangingwall block rotating along strike (D). (D) At any point on the hangingwall surface rotation will result in relative uplift of the hangingwall towards the left side of that point in the diagram and a relative increase in the footwall/hangingwall height relation towards the right side of it. Given the right geomorphic conditions this can induce the erosion of the uplifted portions and inception of alluvial systems. A hypothetical catchment section is shown with a dotted line. No scale implied.

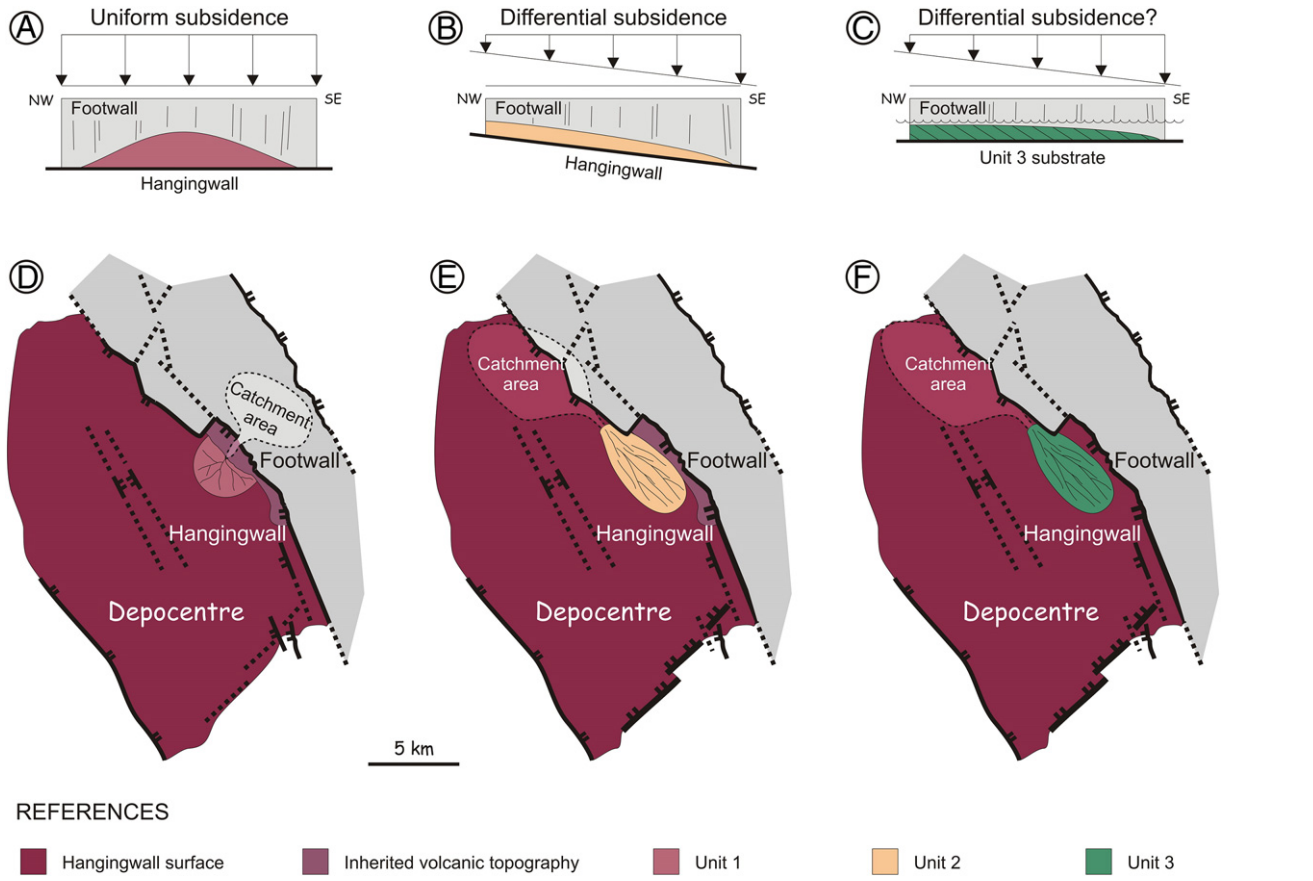

Fig. 15. Hangingwall schematic cross-sections, not to scale, parallel to the border fault system, for Unit 1 depositional times (A), for Unit 2 depositional times (B), and for Unit 3 depositional times (C). Note the different subsidence patterns experienced by the hangingwall between (A) on the one side and (B) on the other side. (C) Deposition of Unit 3 fan delta occurred over a relatively flat substrate on a shallow marine environment. (D), (E) and (F) Paleogeographic representations of Units 1, 2 and 3 sedimentary systems in the rift depocentre. (D) Unit 1 was deposited by a debris flow dominated alluvial system that built a transverse footwall-fed fan with a catchment area situated on the footwall block. (E) Unit 2 was deposited by a hyperconcentrated flow dominated alluvial system that built a hangingwall-fed fan, parallel to the border fault. The catchment area was mainly situated on the hangingwall, with a minor proportion on the footwall. (F) Unit 3 is also the result of hyperconcentrated flow dominated deposition by a hangingwall-fed alluvial system, parallel to the border fault. In this last case, a fan delta was built and the catchment area was fully situated on the hangingwall block. The kink in the northeastern border fault system in (D), (E) and (F) is a possible interpretation that results from reconstructing a portion of that fault system that is now covered by Cenozoic volcanic rocks (Compare with Fig. 3A).

between them in an already linked border fault system commonly occur (e.g., Morley, 2002; Bull et al., 2006). Therefore, the two main possible mechanisms to induce the southeastward rotation of the hangingwall block between deposition of Units 1 and 2 are by increasing the displacement along-strike the northeastern border fault system, and/or by allowing the displacement along the southeastern border fault system to overpass that one along the northeastern border fault system. Due to the inversion of the extensional structures of the Catán-Lil Depocentre the original extensional kinematic indicators were erased or over-printed, precluding any proper kinematic analysis of the fault population. The original geometry of the depocentre and its structures can only be reconstructed from the analysis of the syn-rift stratigraphy (see Section 3). Examination of other depositional systems postdating the lava flow units and from a different location in the Catán-Lil depocentre shows paleoflow directions compatible with the existence of southeast surface gradients in the hangingwall blocks (Muravchik, 2009). As no transverse structures are observed along the northeastern border fault system, it is interpreted that no significant differences in displacement between the fault segments existed during deposition of the alluvial succession (e.g., Schlische, 1992; Anders and Schlische, 1994; Schlische and Anders, 1996; Morley, 1999, 2002). Consequently, increased displacement along the southeastern border fault system is the preferred explanation for the origin of southeastward tilting hangingwall blocks in the Catán-Lil depocentre.

The existence of varied and contrasting directions in the arrangement of extensional structures during the rifting phase of the Neuquén Basin is a well recognised characteristic throughout the basin, interpreted to be caused by a non-unidirectional stress field (e.g., Franzese and Spalletti, 2001; Cristallini et al., 2009; Giambiagi et al., 2009). As such, the half-grabens in the subsurface show a predominant NE–SW polarity in the Neuquén Embayment (eastern Neuquén Basin, Cristallini et al., 2009) and N–S to NW–SE polarities in the Huincul High (southern Neuquén Basin, Vergani, 2005; Fig. 1A,B). W–NW and NE orientated structures are observed to cut the predominant NW border fault systems in the half-grabens from the Neuquén Embayment and oblique rifting is regarded as a possible mechanism (Cristallini et al., 2009). Likewise, the coexistence of both NE–SW and NW–SE directions of extension was identified from kinematic analysis of exposed depocentres from the northern Neuquén Basin (Atuel, Malargüe and Cara Cura-Reyes depocentres) and oblique rifting was proposed for their formation (Giambiagi et al., 2009). Situated immediately to the southeast of the Catán-Lil Depocentre, the Sierra de Chacaico half-graben has N–S polarity and is interpreted as an exposed portion of the Huincul High structure which lies to the east in the subsurface (Franzese et al., 2007; Fig. 1A,B). Consequently the southeastward rotation of the hangingwall block in this case does not necessarily imply any change in the stress field during deposition of the studied succession. On the contrary, the existence of a non-unidirectional stress field and the effects of oblique rifting allow for the development of multiple extensional components that consequently derive in contrasting subsiding patterns through time even in one single depocentre.

7.3. Possible drainage configurations

The existence of an axial fluvial system connecting different depocentres along an extensional fault array is a common feature in basins in a relatively advanced phase of fault growth and linkage and with well integrated drainage networks such as in the Basin and Range, Central Greece and East African Rift (e.g., Jackson and Leeder, 1994; Eliet and Gawthorpe, 1995; Morley, 1999; Densmore et al., 2004). This was not the case for the southwestern Neuquén Basin during deposition of the Precuyano Cycle, when depocentres were isolated entities rarely exceeding 15–20 km in length (Franzese and Spalletti, 2001; Franzese et al., 2006, 2007; D'Elia et al., 2012). There is no evidence of axial fluvial drainage in any of the exposed depocentres, and no other records exist of deposits rich in basement-derived clasts (Franzese et al., 2006, 2007; D'Elia et al., 2012). Precuyano Cycle depocentres are interpreted as relatively isolated drainage basins controlled by the interaction between volcanism and extensional tectonics (Muravchik et al., 2011; D'Elia et al., 2012).

Drainage evolution studies in rift basins are mainly focused on extensive (20–40 km wide and >60 km long) domino-like footwall blocks (Jackson and Leeder, 1994; Ellis et al., 1999; Densmore et al., 2003, 2004, 2005; Cowie et al., 2006). In such areas, large drainage catchments form at the expense of antecedent drainage and/or existence of low relief transfer zones (e.g., Gordon and Heller, 1993; Gawthorpe et al., 1994; Eliet and Gawthorpe, 1995) or due to the structural evolution inherent to extensional fault arrays (Cowie et al., 2006). Footwall uplift is an essential component in the inception of drainage catchments on the footwall block (e.g., Cowie et al., 2006). Uplift results from elastic rebound during seismic slip events (Stein and Barrientos, 1985) and isostatic adjustment to unloading of the footwall block (Jackson and McKenzie, 1983) as well as from the back-tilting of domino-like fault blocks (Jackson et al., 1988). Given the particular horst geometry and dimensions (~5 km across-strike) of the current footwall block, no significant footwall uplift can be expected by those mentioned mechanisms. The existence of large hinterland catchments (sensu Cowie et al., 2006) thus is unrealistic for this case. In this context, the footwall catchment draining into Unit 1 transverse fan is interpreted as a relatively small frontal catchment (sensu Cowie et al., 2006) (Fig. 15D).

The longitudinal alluvial fan represented by Units 2 and 3 deposits implies a catchment area situated to the northwest. According to facies composition the catchment area should have been located mainly on the hangingwall block (Fig. 15E,F). Granitic clast content decreases upwards from 37% at the base to only 8% at the top of Unit 2 until its complete disappearance in Unit 3 (Fig. 6, Log 4). This gradual diminution in the contribution of basement-derived clasts implies variations in the configuration of the drainage network. The catchment area necessarily loses the influence of granite outcrops and becomes volumetrically richer in volcanic rocks. The drainage network became progressively isolated from the footwall blocks, and as such, is interpreted as being mainly endorheic (Fig. 15E,F).

7.4. Footwall to hangingwall drainage shift

As noted above, alluvial fan configuration can be an indicator of the hangingwall slope orientation. Nevertheless, drainage in the catchment area on the footwall block cannot be completely reconstructed from the alluvial fan orientation alone. The boundary surface between Units 1 and 2 is sharp and abrupt, suggesting a sudden shift from one sedimentary system to the other. Abandonment of frontal catchment (sensu Cowie et al., 2006) sourced alluvial fans is a common phenomenon originated by an increase in the displacement of a border fault system (e.g., Seger and Alexander, 1993; Eliet and Gawthorpe, 1995; Cowie et al., 2006). Increased displacement steepens the area around the fault scarps, eventually overcoming the capacity of the drainage system to keep pace by eroding into the footwall block (e.g., Cowie et al., 2006). Also, footwall uplift and back tilting can deflect drainage around the fault segments or simply reverse their course (e.g., Seger and Alexander, 1993; Eliet and Gawthorpe, 1995; Cowie et al., 2006). No transitional deposits that could be assigned either to drainage diversion into the same depocentre or into the contiguous depocentre to the northeast of the footwall block horst were found exposed (Franzese et al., 2006; Muravchik, 2009). The exact reasons why the footwall sourced drainage feeding Unit 1 fan was shut off and replaced by a hangingwall sourced one building Unit 2 and later Unit 3 fans cannot be fully established from the preserved exposures and this matter should remain open to question.

8. Conclusions

A succession of three different alluvial systems was deposited along the border fault of the Catán Lil half-graben in the Neuquén Basin: a transverse footwall-fed alluvial fan dominated by debris flow deposition (Unit 1), a longitudinal hangingwall-fed alluvial fan dominated by hyperconcentrated flow deposition (Unit 2) and a longitudinal hangingwall-fed fan delta dominated by hyperconcentrated flow deposition (Unit 3). Hangingwall rotation is proposed as the main structural control over the orientation of the fans along this half-graben border fault system.

Alluvial fan/fan delta configuration is a sensitive indicator of hangingwall paleoslope direction. Coupled provenance and geometrical analysis of the alluvial successions proved to be essential in order to establish the original orientations of the alluvial systems in the depocentre. The results obtained are especially meaningful for understanding the alluvial evolution in hydrologically closed rift depocentres, where fluvial systems are not very well developed. Correct identification of fan morphology and orientation can provide the only evidence for reconstructing the original drainage pattern in a fossil rift depocentre.

Acknowledgements

M. Muravchik was granted a PhD scholarship by the Consejo Nacional de Investigaciones Científicas y Técnicas de la República Argentina (CONICET). His PhD project was supported by research grants from Agencia Nacional de Promoción Científica y Tecnológica (PICT 07-8451 and 25304). Alejandro Dajil, Laura Lamarca, Nicolás Sandoval, Martín Griffin, Irene Hernando and Mariano Hernández are acknowledged for their assistance in the field and friendship. Marta Pesqueira and Oscar Isasi are specially thanked for their hospitality. Elsa Martínez, her son Juan, and the rest of the people working at Estancia Martínez are acknowledged for allowing us access to the outcrops and for their hospitality. Gonzalo D. Veiga and Rob L. Gawthorpe are thanked for early discussions. Catherine Hunt, Rob L. Gawthorpe and Miguel Griffin provided invaluable help on language editing. Jasper Knight, M. Nieves Meléndez Hevia, C.A. Benavente and an anonymous reviewer are greatly appreciated for the corrections made to the original manuscript.

References

Alexander, J., Leeder, M.R., 1987. Active tectonic control on alluvial architecture. In: Ethridge, F.G., Flores, R.M., Harvey, M.D. (Eds.), Recent Developments in Fluvial Sedimentology. SEPM Special Publication, 39. SEPM, Tulsa, OK, pp. 243–252.

Alexander, J., Leeder, M.R., 1990. Geomorphology and surface tilting in an active extensional basin, SW Montana, USA. Journal of the Geological Society of London 147, 461–467.

Anders, M.H., Schlische, R.W., 1994. Overlapping faults, intrabasin highs, and the growth of normal faults. Journal of Geology 102, 165–179.

Blair, T.C., 1999a. Sedimentary processes and facies of the waterlaid Anvil Spring Canyon alluvial fan, Death Valley, California. Sedimentology 46, 913–940.

Blair, T.C., 1999b. Cause of dominance by sheetflood vs. debris-flow processes on two adjoining alluvial fans, Death Valley, California. Sedimentology 46, 1015–1028.

Blair, T.C., 1999c. Sedimentology of the debris-flow-dominated Warm Spring Canyon alluvial fan, Death Valley, California. Sedimentology 46, 941–965.

Blair, T.C., McPherson, J.G., 1992. The Trollheim alluvial fan facies model revisited. Geological Society of America Bulletin 104, 762–769.

Blair, T.C., McPherson, J.G., 1994. Alluvial fans and their natural distinction from rivers based on morphology, hydraulic processes, sedimentary processes, and facies assemblages. Journal of Sedimentary Research 64, 450–489.
Blair, T.C., McPherson, J.G., 1998. Recent debris-flow processes and resultant form and facies of the Dolomite alluvial fan, Owens Valley, California. Journal of Sedimentary Research 68, 800–818.
Blair, T.C., McPherson, J.G., 2008. Quaternary sedimentology of the Rose Creek fan delta, Walker Lake, Nevada, USA, and implications to fan-delta facies models. Sedimentology 55, 579–615.
Bull, J.M., Barnes, P.M., Lamarche, G., Sanderson, D.J., Cowie, P.A., Taylor, S.K., Dix, J.K., 2006. High-resolution record of displacement accumulation on an active normal fault: implications for models of slip accumulation during repeated earthquakes. Journal of Structural Geology 28, 1146–1166.
Cattaneo, A., Steel, R.J., 2003. Transgressive deposits: a review of their variability. Earth-Science Reviews 62, 187–228.
Cowie, P.A., Attal, M., Tucker, G.E., Whittaker, A.C., Naylor, M., Ganas, A., Roberts, G.P., 2006. Investigating the surface process response to fault interaction and linkage using a numerical modelling approach. Basin Research 18, 231–266.
Cristallini, E., Tomezzoli, R., Pando, G., Gazzera, C., Martínez, J.M., Quiroga, J., Buhler, M., Bechis, F., Barredo, S., Zambrano, O., 2009. Controles pre-cuyanos en la estructura de la Cuenca Neuquina. Revista de la Asociación Geológica Argentina 65, 248–264.
Dasgupta, P., 2003. Sediment gravity flow — the conceptual problems. Earth-Science Reviews 62, 265–281.
D'Elia, L., Muravchik, M., Franzese, J.R., López, L., 2012. Tectonostratigraphic analysis of the Late Triassic–Early Jurassic syn-rift sequence of the Neuquén Basin in the Sañicó depocentre, Neuquén Province, Argentina. Andean Geology 39, 133–157.
D'Elia, L., Martí, J., 2013. Caldera events in a rift depocentre: an example from the Jurassic Neuquén basin, Argentina. Journal of the Geological Society of London 170, 571–584.
Densmore, A.L., Dawers, N.H., Gupta, S., Allen, P.A., Gilpin, R., 2003. Landscape evolution at extensional relay zones. Journal of Geophysical Research - Solid Earth 108 (B5), 2273–2287.
Densmore, A.L., Dawers, N.H., Gupta, S., Guidon, R., Goldin, T., 2004. Footwall topographic development during continental extension. Journal of Geophysical Research - Solid Earth 109 (F0), 3001–3016.
Densmore, A.L., Dawers, N.H., Gupta, S., Guidon, R., 2005. What sets topographic relief in extensional footwalls? Geology 33, 453–456.
Digregorio, J.H., Uliana, M.A., 1980. Cuenca Neuquina. In: Turner, J.C.M. (Ed.), Geología Regional Argentina. Academia Nacional de Ciencias, Córdoba, pp. 985–1032.
Eliet, P.P., Gawthorpe, R.L., 1995. Drainage development and sediment supply within rifts, examples from the Sperchios basin, central Greece. Journal of the Geological Society of London 152, 883–893.
Ellis, M.A., Densmore, A.L., Anderson, R.S., 1999. Development of mountainous topography in the Basin Ranges, USA. Basin Research 11, 21–41.
Fernández, O., Roca, E., Muñoz, J.A., 2003. Projection of dip data in conical folds onto a cross-section plane. Journal of Structural Geology 25, 1875–1882.
Franzese, J.R., Spalletti, L.A., 2001. Late Triassic–Early Jurassic continental extension in southwestern Gondwana: tectonic segmentation and pre-break-up rifting. Journal of South American Earth Sciences 14, 257–270.
Franzese, J.R., Veiga, G.D., Schwarz, E., Gómez-Pérez, I., 2006. Tectonostratigraphic evolution of a Mesozoic graben border system: the Chachil depocentre, southern Neuquén Basin, Argentina. Journal of the Geological Society of London 163, 707–721.
Franzese, J.R., Veiga, G.D., Muravchik, M., Ancheta, D., D'Elia, L., 2007. Estratigrafía de 'sin-rift' (Triásico Superior-Jurásico Inferior) de la Cuenca Neuquina en la sierra de Chacaico, Neuquén, Argentina. Revista Geologica de Chile 34, 49–62.
Gawthorpe, R.L., Hurst, J.M., 1993. Transfer zones in extensional basins: their structural style and influence on drainage development and stratigraphy. Journal of the Geological Society of London 150, 1137–1152.
Gawthorpe, R.L., Fraser, A.J., Collier, E.L., 1994. Sequence stratigraphy in active extensional basins: implications for the interpretation of ancient basin-fills. Marine and Petroleum Geology 11, 642–658.
Gawthorpe, R.L., Leeder, M.R., 2000. Tectono-sedimentary evolution of active extensional basins. Basin Research 12, 195–218.
Giambiagi, L., Bechis, F., Lanés, S., Tunik, M., García, V., Suriano, J., Mescua, J., 2008. Formación y evolución triásico - jurásica del depocentro Atuel, Cuenca Neuquina, provincia de Mendoza. Revista de la Asociación Geológica Argentina 63, 520–533.
Giambiagi, L.B., Tunik, M., Barredo, S., Bechis, F., Ghiglione, M., Alvarez, P., Drosina, M., 2009. Cinemática de apertura del sector norte de la cuenca Neuquina. Revista de la Asociación Geológica Argentina 65, 278–292.
Gordon, I., Heller, P.L., 1993. Evaluating major controls on basinal stratigraphy, Pine Valley, Nevada: implications for syntectonic deposition. Geological Society of America Bulletin 105, 47–55.
Groeber, P., 1946. Observaciones geológicas a lo largo del meridiano 70, Hoja Chos Malal. Revista de la Asociación Geológica Argentina 1, 177–208.
Groeber, P., 1956. Acerca de la edad del Sañicolitense. Revista de la Asociación Geológica Argentina 11, 67–98.
Gulisano, C.A., 1981. El ciclo cuyano en el norte de Neuquén y sur de Mendoza. VIII Congreso Geológico Argentino, 3, pp. 579–592.
Gulisano, C.A., Pando, G.A., 1981. Estratigrafia y facies de los depositos jurasicos entre Piedra del Aguila y Sanico, Departamento Collon Cura, Provincia del Neuquén. VIII Congreso Geológico Argentino, 3, pp. 553–577.
Gulisano, C.A., Gutiérrez Pleimling, A.R., Digregorio, R.E., 1984. Esquema estratigráfico de la secuencia jurásica del oeste de la provincia del Neuquén. IX Congreso Geológico Argentino. , 1, pp. 236–259.
Howell, J.A., Schwarz, E., Spalletti, L.A., Veiga, G.D., 2005. The Neuquén Basin: an overview. In: Veiga, G.D., Spalletti, L.A., Howell, J.A., Schwarz, E. (Eds.), The Neuquén Basin, Argentina: A Case Study in Sequence Stratigraphy and Basin Dynamics. Geological Society Special Publication, 252. Blackwell, London, pp. 1–14.
Jackson, J.A., Leeder, M.R., 1994. Drainage systems and the development of normal faults: an example from Pleasant Valley, Nevada. Journal of Structural Geology 16, 1041–1059.
Jackson, J.A., McKenzie, D., 1983. The geometrical evolution of normal fault systems. Journal of Structural Geology 5, 471–482.
Jackson, J.A., White, N.J., Garfunkel, Z., Anderson, H., 1988. Relations between normal-fault geometry, tilting and vertical motions in extensional terrains: an example from the southern Gulf of Suez. Journal of Structural Geology 10, 155–170.
Lanés, S., 2005. Late Triassic to Early Jurassic sedimentation in northern Neuquén Basin, Argentina: tectosedimentary evolution of the first transgression. Geologica Acta 3, 81–106.
Leanza, H.A., 1990. Estratigrafía del Paleozoico y Mesozoico anterior a los Movimientos Intermálmicos en la comarca del Cerro Chachil, provincia del Neuquén. Revista de la Asociación Geológica Argentina 45, 272–299.
Leeder, M.R., Gawthorpe, R.L., 1987. Sedimentary models for extensional tilt-block/half-graben basins. In: Coward, M.P., Dewey, J.F., Hancock, P.L. (Eds.), Continental Extensional Tectonics, Geological Society Special Publication 28. Blackwell, London, pp. 139–152.
Leeder, M.R., Jackson, J.A., 1993. The interaction between normal faulting and drainage in active extensional basins, with examples from the western United States and central Greece. Basin Research 5, 79–102.
Leeder, M.R., Mack, G.H., 2001. Lateral erosion ('toe-cutting') of alluvial fans by axial rivers: implications for basin analysis and architecture. Journal of the Geological Society of London 158, 885–893.
Leeder, M.R., Mack, G.H., Salyards, S.L., 1996. Axial-transverse fluvial interactions in half-graben: Plio-Pleistocene Palomas Basin, southern Río Grande Rift, New Mexico, USA. Basin Research 12, 225–241.
Legarreta, L., Uliana, M.A., 1996. The Jurassic succession in west-central Argentina: stratal patterns, sequences and paleogeographic evolution. Palaeogeography, Palaeoclimatology, Palaeoecology 120, 303–330.
Mack, G.H., Leeder, M.R., 1999. Climatic and tectonic controls on alluvial-fan and axial-fluvial sedimentation in the Plio-Pleistocene Palomas half graben, Southern Rio Grande Rift. Journal of Sedimentary Research 69, 635–652.
McPherson, J.G., Shanmugam, G., Moiola, R.J., 1987. Fan-deltas and braid deltas: varieties of coarse grained deltas. Geological Society of America Bulletin 99, 331–340.
Morley, C.K., 1999. Patterns of displacement along large normal faults: implications for basin evolution and fault propagation, based on examples from East Africa. AAPG Bulletin 83, 613–634.
Morley, C.K., 2002. Evolution of large normal faults: evidence from seismic reflection data. AAPG Bulletin 86, 961–978.
Mortimer, E., Gupta, S., Cowie, P.A., 2005. Clinoform nucleation and growth in coarse-grained deltas, Loreto basin, Baja California Sur, Mexico: a response to episodic accelerations in fault displacement. Basin Research 17, 337–359.
Muravchik, M., 2009. Controles estructurales y volcánicos sobre las secuencias de sin-rift (Precuyano) de la Cuenca Neuquina. (PhD Thesis) Universidad Nacional de La Plata, Argentina (291 pp.).
Muravchik, M., D'Elia, L., Bilmes, A., Franzese, J.R., 2011. Syn-eruptive/inter-eruptive relations in the syn-rift deposits of the Precuyano Cycle, Sierra de Chacaico, Neuquén Basin, Argentina. Sedimentary Geology 238, 132–144.
Nichols, G., Thompson, B., 2005. Bedrock lithology control on contemporaneous alluvial fan facies, Oligo-Miocene, southern Pyrenees, Spain. Sedimentology 52, 571–585.
Orton, G.J., Reading, H.G., 1993. Variability of deltaic processes in terms of sediment supply, with particular emphasis on grain size. Sedimentology 40, 475–512.
Peakall, J., Leeder, M.R., Best, J., Ashworth, P., 2000. River response to lateral ground tilting: a synthesis and some implications for the modelling of alluvial architecture in extensional basins. Basin Research 12, 413–424.
Postma, G., 1990. Depositional architecture and facies of river and fan deltas: a synthesis. In: Colella, A., Prior, D.B. (Eds.), Coarse-Grained Deltas. IAS Special Publication, 10, pp. 13–27.
Riccardi, A.C., Damborenea, S., Manceñido, M., Scasso, R., Lanés, S., Iglesia Llanos, M., 1997. Primer registro de Triásico marino fosilífero de la Argentina. Revista de la Asociación Geológica Argentina 52, 228–234.
Roberts, S., Jackson, J.A., 1991. Active normal faulting in central Greece: an overview. In: Roberts, A.M., Yielding, G., Freeman, B. (Eds.), The Geometry of Normal Faults. Geological Society Special Publication, 56. Blackwell, London, pp. 125–142.
Schlische, R.W., 1992. Structural and stratigraphic development of the Newark extensional basin, eastern North America: evidence for the growth of the basin and its bounding structures. Geological Society of America Bulletin 104, 1246–1263.
Schlische, R.W., Anders, M.H., 1996. Stratigraphic effects and tectonic implications of the growth of normal faults and extensional basins. In: Beratan, K.K. (Ed.), Reconstructing the History of Basin and Range Extension Using Sedimentology and Stratigraphy. Special Paper of the Geological Society of America, 303. Boulder, pp. 183–203.
Seger, M., Alexander, J., 1993. Distribution of Plio-Pleistocene and modern coarse-grained deltas south of the Gulf of Corinth, Greece. In: Frostick, L.E., Steel, R.J. (Eds.), Tectonic Controls and Signatures in Sedimentary Successions. IAS Special Publication, 20, pp. 37–48.
Smith, G.A., 1986. Coarse-grained nonmarine volcaniclastic sediment — terminology and depositional process. Geological Society of America Bulletin 97, 1–10.
Stein, R.S., Barrientos, S.E., 1985. Planar high-angle faulting in the Basin and Range: geodetic analysis of the 1983 Borah Peak, Idaho, Earthquake. Journal of Geophysical Research - Solid Earth 90, 11355–11366.
Sohn, Y.K., Son, M., 2004. Synrift stratigraphic geometry in a transfer zone coarse-grained delta complex, Miocene Pohang Basin, SE Korea. Sedimentology 51, 1387–1408.

Tankard, A.J., Uliana, M.A., Welsink, H.J., Ramos, V.A., Turic, M., França, A.B., Milani, E.J., de Brito Neves, B.B., Eyles, N., Skarmeta, J., Santa Ana, H., Wiens, F., Cirbián, M., López, P.O., Germs, G.J.B., De Wit, M.J., Machacha, T., Miller, R.McG., 1995. Tectonic controls of basin evolution in southwestern Gondwana. In: Tankard, A.J., Suárez, S.R., Welsink, H.J. (Eds.), Petroleum Basins of South America. American Association Petroleum Geology Memoir, 62, pp. 5–52.

Uliana, M., Legarreta, L., 1993. Hydrocarbons habitat in a Triassic-to-Cretaceous sub-Andean setting: Neuquén Basin, Argentina. Journal of Petroleum Geology 16, 397–420.

Vergani, G.D., 2005. Control estructural de la sedimentación jurásica (Grupo Cuyo) en la Dorsal de Huincul, Cuenca Neuquina, Argentina. Modelo de falla lístrica rampa-plano, invertida. Boletín de Informaciones Petroleras 1, 32–42.

Vergani, G.D., Tankard, A.J., Belotti, H.J., Weisink, H.J., 1995. Tectonic evolution and paleogeography of the Neuquén basin, Argentina. In: Tankard, A.J., Suárez, S.R., Welsink, H.J. (Eds.), Petroleum Basins of South America. American Association Petroleum Geology Memoir, 62, pp. 382–402.

Wagreich, M., Strauss, P.E., 2005. Source area and tectonic control on alluvial-fan development in the Miocene Fohnsdorf intramontane basin, Austria. In: Harvey, A.M., Mather, A.E., Stokes, M. (Eds.), Alluvial Fans: Geomorphology, Sedimentology, Dynamics. Geological Society Special Publication, 251. Blackwell, London, pp. 207–216.

Weaver, C.E., 1931. Paleontology of the Jurassic and Cretaceous of West Central Argentina. Memoir University of Washington 1, 1–469.